การป้องกันสนามแม่เหล็กโลก
สำหรับหอสังเกตการณ์นิวตริโนใต้ดินเจียงเหมิน

นายจุลนันทน์ ทรงวัฒนา

วิทยานิพนธ์นี้เป็นส่วนหนึ่งของการศึกษาตามหลักสูตรปริญญาวิทยาศาสตรมหาบัณฑิต
สาขาวิชาฟิสิกส์
มหาวิทยาลัยเทคโนโลยีสุรนารี
ปีการศึกษา 2560

THE EARTH MAGNETIC FIELD SHIELDING FOR JIANGMEN UNDERGROUND NEUTRINO OBSERVATORY

Julanan Songwadhana

A Thesis Submitted in Partial Fulfillment of the Requirements for the

Degree of Master of Science in Physics

Suranaree University of Technology

Academic Year 2017

THE EARTH MAGNETIC FIELD SHIELDING FOR JIANGMEN UNDERGROUND NEUTRINO OBSERVATORY

Suranaree University of Technology has approved this thesis submitted in partial fulfillment of the requirements for a Master's Degree.

Thesis Examining Committee

(Dr. Nuanwan Sanguansak)
Chairperson

(Dr. Khanchai Khosonthongkee)
Member (Thesis Advisor)

(Prof. Dr. Yupeng Yan)
Member

(Asst. Prof. Dr. Ayut Limphirat)
Member

(Prof. Dr. Santi Maensiri)
Vice Rector for Academic Affairs and Internationalization

(Asst. Prof. Dr. Worawat Meevasana)
Dean of Institute of Science

จุลนันทน์ ทรงวัฒนา : การป้องกันสนามแม่เหล็กโลกสำหรับหอสังเกตการณ์นิวตริโนใต้ดินเจียงเหมิน (THE EARTH MAGNETIC FIELD SHIELDING FOR JIANGMEN UNDERGROUND NEUTRINO OBSERVATORY) อาจารย์ที่ปรึกษา : อาจารย์ ดร. ขรรค์ชัย โกศลทองกี่ , 107 หน้า

งานวิจัยนี้มีจุดประสงค์เพื่อการศึกษาประสิทธิภาพการป้องกันสนามแม่เหล็กโลกของแบบจำลองขดลวดในรูปแบบต่าง ๆ สำหรับเครื่องตรวจวัดของหอสังเกตการณ์นิวตริโนใต้ดินเจียงเหมิน (JUNO) ในการวิจัยได้การประยุกต์ใช้การหาปริพันธ์เชิงตัวเลขโดยวิธีการประมาณเกาส์-เลอช็องดร์ผ่านการเขียนโปรแกรมด้วยภาษาฟอร์แทรน 77 ในขณะที่ การหาค่าที่เหมาะสมที่สุดของกระแสไฟฟ้าในขดลวดใช้วิธีกำลังสองน้อยที่สุดแบบตัวแปรมีขอบเขตด้วยการเขียนโปรแกรมภาษาไพทอน จากการศึกษาพบว่าแบบจำลองขดลวดเพียงหนึ่งชุดจำนวน 32 ขดมีความเหมาะสม โดยแบบจำลองดังกล่าวสามารถป้องกันสนามแม่เหล็กโลกให้มีค่าสนามแม่เหล็กสุทธิต่ำกว่าร้อยละ 10 ในบริเวณหลอดโฟโตมัลติพลายเออร์ซึ่งติดตั้งบริเวณตัวตรวจจับกลาง และ ต่ำกว่าร้อยละ 15 ในบริเวณหลอดโฟโตมัลติพลายเออร์ซึ่งติดตั้งบริเวณตัวตรวจจับยับยั้ง งานวิจัยนี้ยังแสดงให้เห็นว่าผลกระทบ ของความคลาดเคลื่อนที่เป็นไปได้ในการติดตั้งขดลวดมีเพียงเล็กน้อย แต่ผลกระทบของความโน้มเอียงของสนามแม่เหล็กโลกในอีก 20 ปีข้างหน้าอาจส่งผลกระทบอย่างมีนัยสำคัญต่อประสิทธิภาพของหลอดโฟโตมัลติพลายเออร์

สาขาวิชาฟิสิกส์ ลายมือชื่อนักศึกษา จุลนันทน์ ทรงวัฒนา

ปีการศึกษา 2560 ลายมือชื่ออาจารย์ที่ปรึกษา

JULANAN SONGWADHANA : THE EARTH MAGNETIC FIELD SHIELDING FOR JIANGMEN UNDERGROUND NEUTRINO OBSERVATORY. THESIS ADVISOR : KHANCHAI KHOSONTHONGKEE, Ph.D. 107 PP.

JUNO/PMT/GAUSS-LEGENDRE QUADRATURE/OPTIMIZATION/COILS SHIELDING/ELECTROMAGNETIC SHIELDING

The work is to study the earth magnetic field shielding efficiency of various coil models for the detectors of JUNO. In the research, the Gauss-Legendre quadrature is applied in the numerical integration with Fortran77 programming while the bounded-variable least squares method is used for the electrical currents optimization with Python programming. It is found that a one-set model of 32 circular coils is very promising, which is able to shield the earth magnetic field to below 10 % in the CD-PMT region and below 15 % in the Veto-PMT region. The work also reveals that the effect of mostly possible installation errors is negligible, but the magnetic inclination may have an sizable impact on the PMT efficiency in 20 years.

School of Physics

Academic Year 2017

Student's Signature _____

Advisor's Signature _____

ACKNOWLEDGEMENTS

I would first like to thank my thesis advisor, Dr.Khanchai Khosonthongkee and my thesis co-advisor, Professor Dr.Yupeng Yan and Assistant Professor Dr.Ayut Limphirat of the School of Physics at Suranaree University of Technology for the continuous support and their assistance.

My sincere thanks to all lecturers in the School of Physics who have taught me in academic years, especially Associate Professor Dr.Sirichok Jungthawan. I have developed my computational skill and my research with his help.

I would like to thank all experts in IHEP for providing a residence at IHEP and guiding me about my research during my life in China.

Heartfelt thanks go to Institute of Research and Development (IRD) at Suranaree University of Technology whose gave OROG scholarship to me and the Center for Computer Services at Suranaree University of Technology for furnishing the computing resource.

I also would like to thank the Beamline 1.3 at Synchrotron Light Research Institute (SLRI) to hire me as a part-time student and give a good opportunity to help the researchers in operating those experiments.

Finally, I would like to express my very profound gratitude to my parents for continuous encouragement during my years of study and pass the process of researching and writing this dissertation. This achievement would have been impossible without them. Thank you.

Julanan Songwadhana

CONTENTS

CONTENTS (Continued)

Page

CONTENTS (Continued)

Page

LIST OF TABLES

LIST OF TABLES (Continued)

LIST OF FIGURES

LIST OF FIGURES (Continued)

LIST OF FIGURES (Continued)

LIST OF FIGURES (Continued)

LIST OF FIGURES (Continued)

LIST OF ABBREVIATIONS

AS	Acrylic Sphere
BVLS	Bounded-Variable Least Squares Method
CD	Central Detector
CPV	Charge Parity Violation
DC	Direct Current
EMF	The Earth Magnetic Field
Gd	Gadolinium
IAGA	International Association of Geomagnetism and Aeronomy
IBD	Invert Beta Decay
IGRF	International Geomagnetic Reference Field
IH	Inverted Hierarchy
IHEP	Institute of High Energy Physics
JUNO	The Jiangmen Underground Neutrino Observatory
KamLAND	The Kamioka Liquid Scintillator Antineutrino Detector
LS	Least Square
MH	Mass Hierarchy
MINOS	The Main Injector Neutrino Oscillation search
NH	Normal Hierarchy
NNLS	Non-Negative Least Squares Method
pe	Photoelectrons

LIST OF ABBREVIATIONS (Continued)

PMNS	Pontecorvo-Maki-Nakagawa-Sakata Matrix
PMT	Photomultiplier Tube
RENO	The Reactor Experiment for Neutrino Oscillations
SSLS	Stainless Steel Latticed Shell
T2K	The Tokai to Kamioka

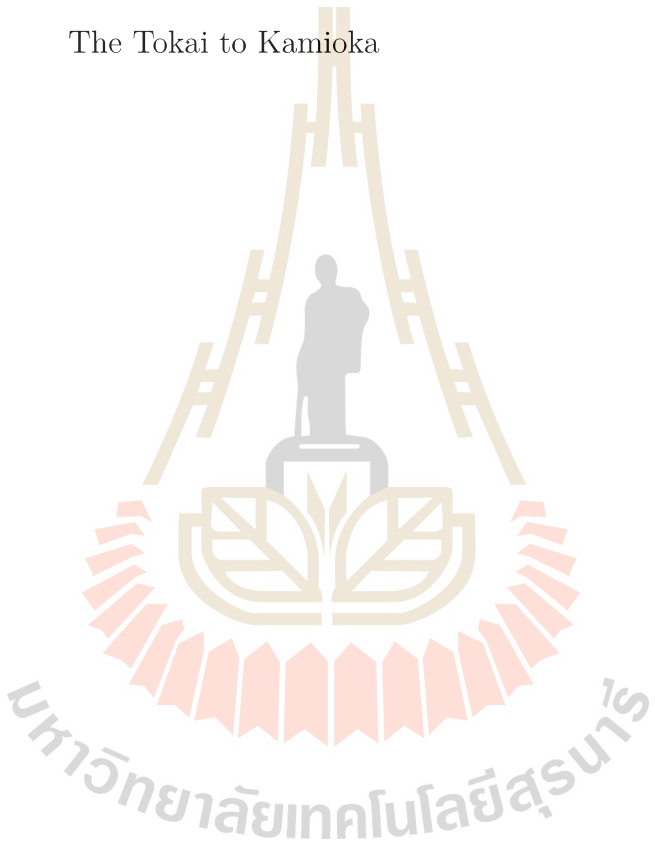

CHAPTER I

INTRODUCTION

In the standard model (SM), elementary particles are sorted according to their spin. These can be grouped in three sectors, two third sectors have half-integer spin, The so-called fermions. Fermions interact with each other via bosons which are classified as integer spin of the SM (Braibant et al., 2012). Two third sectors of the SM compose of six quarks and six leptons. Nine of fermions couple to the electromagnetic interaction while others are able to react only with the weak interaction because their are a neutral charge particle. Moreover, it lacks a conservative with charges or any other quantum number. A particle in previous conditions are neutrino. Neutrinos are three flavors of neutrinos known as electron-neutrino (ν_e), muon-neutrino (ν_μ) and tau-neutrino (ν_τ) and their anti-particle. Left-handed neutrino and right-handed anti-neutrino merely exist in helicity property. This means that the directions of spin and motion is opposite for neutrino, but anti-neutrino has the same directions. Nowadays, only left-handed neutrinos and right-handed antineutrinos are exist experimentally (Goldhaber et al., 1958). Even though neutrinos are taken into account massless according to the SM, plenty of experiments have presented that neutrinos should have a small or non-zero mass. For the discovery of the neutrino oscillation phenomena from early observations, The 2015 Nobel Prize in physics was shared by Takaaki Kajita and Arthur B. McDonald. So, the phenomena has encouraged physicists whose are interesting in the neutrino to study oscillating properties.

1.1 Neutrino mixing and oscillations

The neutrino flavor states or flavor eigenstates ($|\nu_i\rangle$(i=e,μ,τ)) are superpositions of three mass eigenstates ($|\nu_j\rangle$ (j=1, 2, 3)) or can be described in the basis of the mass eigenstates and vice versa with the linear combination

$$|\nu_i\rangle = \sum_{j=1}^{3} U_{ji} |\nu_j\rangle , \tag{1.1}$$

$$|\nu_j\rangle = \sum_{i=1} U_{ji}^{*} |\nu_i\rangle . \tag{1.2}$$

Where unitary matrix (U_{ji}) is the 3×3 unitary neutrino mixing matrix or Pontecorvo-Maki-Nakagawa-Sakata matrix (PMNS) (Schechter and Valle, 1980). Neutrinos may change their flavors during the traveling in consequence of quantum interference. This phenomenon is known as neutrino mixing or neutrino oscillation. Neutrino mixing parameters are coupling in PMNS matrix as the Eq. 1.3.

$$\begin{aligned} U = & \begin{pmatrix} c_{12}c_{13} & s_{12}c_{13} & s_{13}e^{-i\delta} \\ -s_{12}c_{23} - c_{12}s_{23}s_{13}e^{i\delta} & c_{12}c_{23} - s_{12}s_{23}s_{13}e^{i\delta} & s_{23}c_{13} \\ s_{12}s_{23} - c_{12}c_{23}s_{13}e^{i\delta} & -c_{12}s_{23} - s_{12}c_{23}s_{13}e^{i\delta} & c_{23}c_{13} \end{pmatrix} \\ & \times diag\left(1, e^{i\frac{\alpha_{21}}{2}}, e^{i\frac{\alpha_{31}}{2}}\right), \end{aligned} \tag{1.3}$$

where $c_{ij} = \cos(\theta_{ij})$, $s_{ij} = \sin(\theta_{ij})$, the mixing angles $\theta_{ij} = [0, \pi/2]$, the Dirac CP violation phase $\delta = [0, 2\pi]$, α_{21} and α_{31} are two Majorana CP violation (CPV) phases (Patrignani et al., 2016). Intention of neutrino oscillation parameters survey used to explore in appearing the observed matter-antimatter asymmetry in the universe (Abe et al., 2015b). Those parameters are able to be determined via the transition probability, the probability changing neutrino flavor state. The transition probability involves with amplitudes and frequencies of oscillation. Am-

plitudes of oscillation are related to the mixing angles θ_{12}, θ_{23} and θ_{13}. From the formalism of quantum mechanics, the time dependent amplitude of neutrino oscillation is associated with PMNS matrix as the Eq. 1.4,

$$A(\nu_\alpha \to \nu_\beta) = \langle \nu_\beta | \nu_\alpha(t) \rangle = \sum_i U^*_{\alpha i} U_{\beta i} \exp^{-iE_i t} . \tag{1.4}$$

For small neutrino mass, the energy $E_i = \sqrt{p^2 + m_i^2}$ can be approximated as $E + m_i^2/2E$. The probability that an electron antineutrino from a source will be found as an electron antineutrino, the so-called the survival probability, can be written as

$$\begin{aligned} P(\bar{\nu}_e \to \bar{\nu}_e) = 1 - \sin^2(2\theta_{13}) \left[\cos^2(\theta_{12}) \sin^2 \left(\frac{\Delta m^2_{31} L}{4E} \right) + \sin^2(\theta_{12}) \sin^2 \left(\frac{\Delta m^2_{32} L}{4E} \right) \right] \\ - \cos^4(\theta_{13}) \sin^2(2\theta_{12}) \sin^2 \left(\frac{\Delta m^2_{21} L}{4E} \right) , \end{aligned} \tag{1.5}$$

where L is a traveled distance of a neutrino and Δm^2_{ij} are the difference of squared neutrino mass m_i and m_j (Balantekin and Haxton, 2013). Oscillation frequencies are determined by the difference of squared neutrino masses, $\Delta m^2_{ij} = m^2_i - m^2_j$ (Fengpeng et al., 2016). θ_{12} and Δm^2_{21} were measured by KamLAND (Gando et al., 2011). Atmospheric and accelerator neutrino experiments have been using to measure θ_{23} and $|\Delta m^2_{32}|$. The last parameter is mixing angle θ_{13}, which was searched by reactor neutrino experiments at Daya Bay (An et al., 2012), RENO (Ahn et al., 2012), accelerator neutrino experiments T2K (Abe et al., 2011) and MINOS (Adamson et al., 2008). The recent status of neutrino oscillation parameters fit are shown in Table 1.1 (de Salas et al., 2017).

The masses of neutrinos have not been determined yet. Thus, The next generation neutrino oscillation experiments is going to determine the sign of Δm^2_{32} (mass hierarchy), precisely measure all oscillation parameters and search for CP

Table 1.1 Neutrino oscillation parameters summary determined from this global analysis. The ranges for inverted ordering refer to the local minimum of this neutrino mass ordering.

parameter	best fit ± 1σ	2σ range	3σ range
$\Delta m^2_{21}\,[10^{-5}eV^2]$	7.56±0.19	7.20-7.95	7.05-8.14
$\Delta m^2_{31}\,[10^{-3}eV^2]$ (NO)	2.55±0.04	2.47-2.63	2.43-2.67
$\Delta m^2_{31}\,[10^{-3}eV^2]$ (IO)	2.49±0.04	2.41-2.57	2.37-2.61
$\sin^2(\theta_{12})/10^{-1}$	$3.21^{+0.18}_{-0.16}$	2.89-3.59	2.73-3.79
$\theta_{12}/^\circ$	$34.5^{+1.1}_{-1.0}$	32.5-36.8	31.5-38.0
$\sin^2(\theta_{23})/10^{-1}$ (NO)	$4.30^{+0.20}_{-0.18}$ [a]	3.98-4.78 & 5.60-6.17	3.84-6.35
$\theta_{23}/^\circ$	41.0 ± 1.1	39.1-43.7 & 48.4-51.8	38.3-52.8
$\sin^2(\theta_{23})/10^{-1}$ (IO)	$5.96^{+0.17}_{-0.18}$ [b]	4.04-4.56 & 5.56-6.25	3.88-6.38
$\theta_{23}/^\circ$	50.5 ± 1.0	39.5-42.5 & 48.2-52.2	38.5-53.0
$\sin^2(\theta_{13})/10^{-1}$ (NO)	$2.155^{+0.090}_{-0.075}$	1.98-2.31	1.89-2.39
$\theta_{13}/^\circ$	$8.44^{+0.18}_{-0.15}$	8.1-8.7	7.9-8.9
$\sin^2(\theta_{13})/10^{-1}$ (IO)	$2.140^{+0.082}_{-0.085}$	1.97-2.30	1.89-2.39
$\theta_{13}/^\circ$	$8.41^{+0.16}_{-0.17}$	8.0-8.7	7.9-8.9
δ/π (NO)	$1.40^{+0.31}_{-0.20}$	0.85-1.95	0.00-2.00
$\delta/^\circ$	252^{+56}_{-36}	153-351	0-360
δ/π (IO)	$1.44^{+0.26}_{-0.23}$	1.01-1.93	0.00-0.17 & 0.79-2.00
$\delta/^\circ$	259^{+47}_{-41}	182-347	0-31 & 142-360

[a]There is a local minimum in the second octant, at $\sin^2(\theta_{23}) = 0.596$ with $\Delta\chi^2 = 2.08$ with respect to the global minimum.

[b]There is a local minimum in the first octant, at $\sin^2(\theta_{23}) = 0.426$ with $\Delta\chi^2 = 1.68$ with respect to the global minimum for IO.

NO and IO are short for normal and inverted ordering, respectively.

violation in the neutrino oscillation. The determination of neutrino mass hierarchy can answer whether the third mass eigenstate (m_3) be heavier or lighter than the first and second mass eigenstates (m_1, m_2). The neutrino mass hierarchy could be the so-called normal mass hierarchy (NH) and the so-called inverted mass hierarchy (IH) which refer to $m_3 > m_1$ and $m_3 < m_1$, respectively. as shown in Figure 1.1 (Ciuffoli et al., 2013). The mass hierarchy of NH and IH have the relation as the followings:

$$NH : |\Delta m^2_{31}| = |\Delta m^2_{32}| + |\Delta m^2_{21}|, \tag{1.6}$$

$$IH : |\Delta m^2_{31}| = |\Delta m^2_{32}| - |\Delta m^2_{21}|. \tag{1.7}$$

In principle, the neutrino mass hierarchy is determined by accurate measurements of $|\Delta m^2_{31}|$ and $|\Delta m^2_{32}|$. In reality it is very difficult because $|\Delta m^2_{21}|$ is just about 3% of $|\Delta m^2_{32}|$, then $|\Delta m^2_{31}|$ and $|\Delta m^2_{32}|$ have to be measured with a precision better than 3% (Zhan et al., 2008). NH and IH can be discriminated by the energy spectrum of antineutrino as shown in Figure 1.2. The energy spectra pattern is clearly separated in case of NH and IH.

The neutrino mass hierarchy is very important because in the standard model elementary particles are related to each others in their interaction. If we know the MH it may be possible to solve the long standing mystery of why the present universe is filled with only particles and almost without antiparticles. The determination of the mass hierarchy is crucial to understand fundamental laws of physics as well as the evolution of the universe (Abe et al., 2015a).

There are a number of commissioning and under-construction experiments aiming to determine the neutrino mass hierarchy. One of a reactor neutrino experiment is The Jiangmen Underground Neutrino Observatory (JUNO). JUNO is

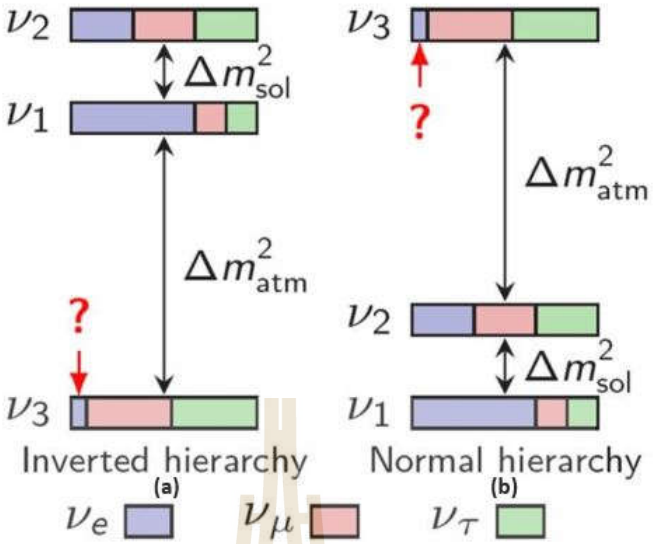

Figure 1.1 The two difference model of mass hierarchy (a) Inverted hierarchy(IH) (b) Normal hierarchy(NH).

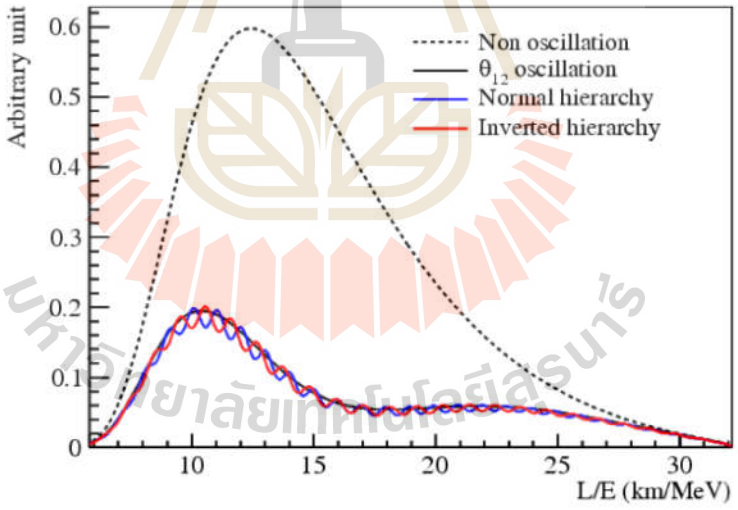

Figure 1.2 The energey spectra pattern of normal hierarchy(blue line) and inverted hierarchy(red line) from reactor neutrino spectra at a baseline of 60 km in L/E space (Zhan et al., 2008).

under construction at Kaiping, Jiangmen in Southern China aims to determine the neutrino mass hierarchy and measures more precisely the PMNS matrix elements.

1.2 JUNO reactor experiment

JUNO is a reactor antineutrino experiment with the main purpose for determining the neutrino mass hierarchy by precisely measuring the energy spectrum of nuclear reactor electron antineutrinos at a distance of 53 kilometers from the reactors (Yangjiang and Taishan nuclear power plants). JUNO is located 700 meters deep underground to reduce cosmogenic muon flux as shown in Figure 1.3 (Lu, 2017). The JUNO consists of a central detector (CD) with 20 kilotons an organic liquid scintillator filling the spherical CD or acrylic sphere whose diameter is 35.4 meters, surrounded by a water pool, approximately $18,000$ $20''$ and $25,000$ $3''$ photomultiplier tubes (PMTs) on the inner CD truss. The liquid scintillator used in JUNO composes of linear alkyl benzene (LAB) as the solvent, 3 g/L 2,5-diphenyloxazole (PPO) as the fluor, and 15 mg/L p-bis-(o-methylstyryl)-benzene (bis-MSB) as the wavelength shifter (Li et al., 2013). An organic material of the liquid scintilltor can be excited by ionizing particles. This material is very efficient in ionization comparing with other materials. Because there can produce approximately 10^4 photons in the near UV and blue per MeV of the deposited energy. $2,400$ $20''$ Veto-PMT are installed on the outer acrylic sphere for colecting cherenkov light. A cursory PMT position are yellow points in Figure 1.4.

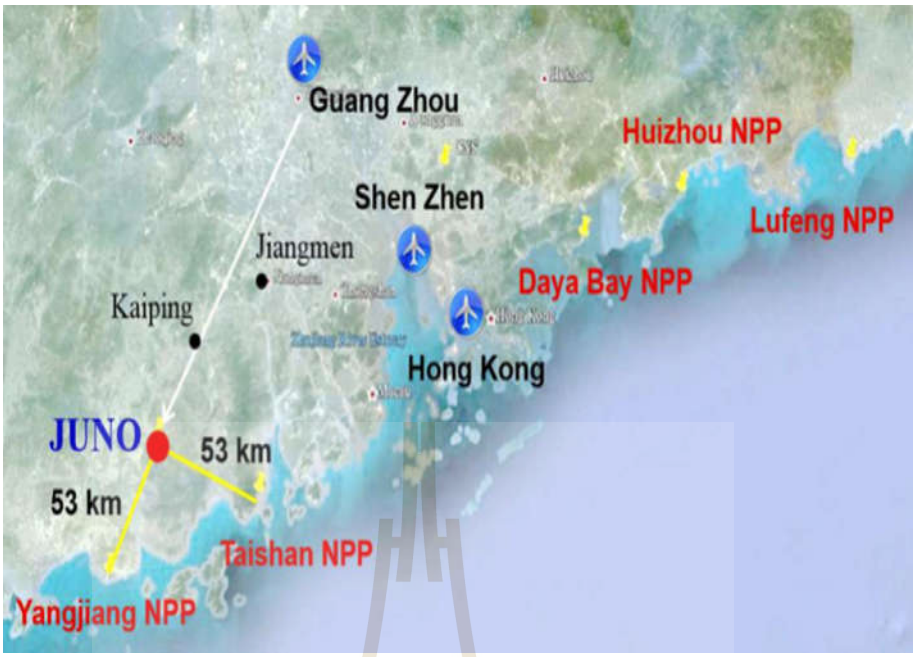

Figure 1.3 The location of Taishan reactor, Yangjiang reactor and JUNO site.

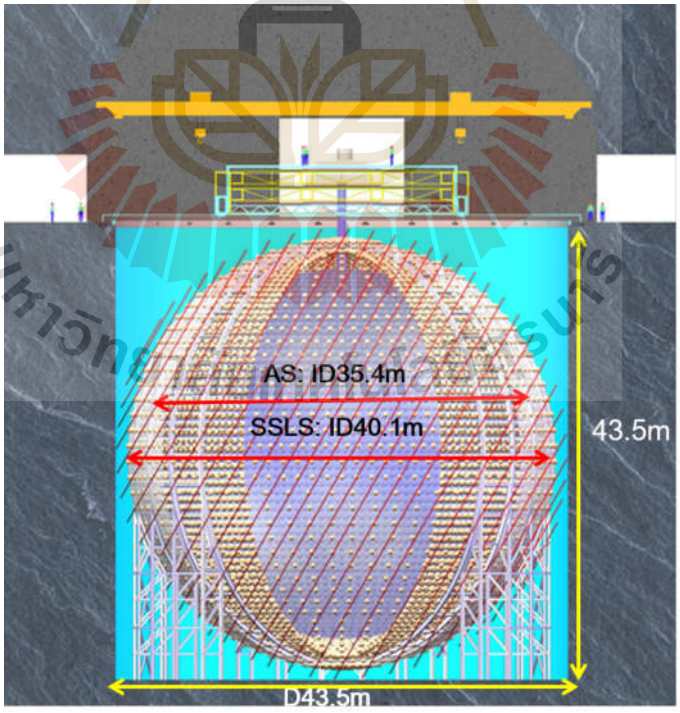

Figure 1.4 JUNO experimental hall model.

The required energy resolution for JUNO detectors to distinguish between the NH and IH is about 3% at 1 MeV. The energy resolution was predicted by simulation as seen in Figure 1.5. The results is grounded on the energy reconstruction of PMT counting with an ideal vertex reconstruction. The JUNO is designed to reach the goal by colecting high light or 1200 photoelectrons (pe) per 1 MeV (Jollet, 2017).

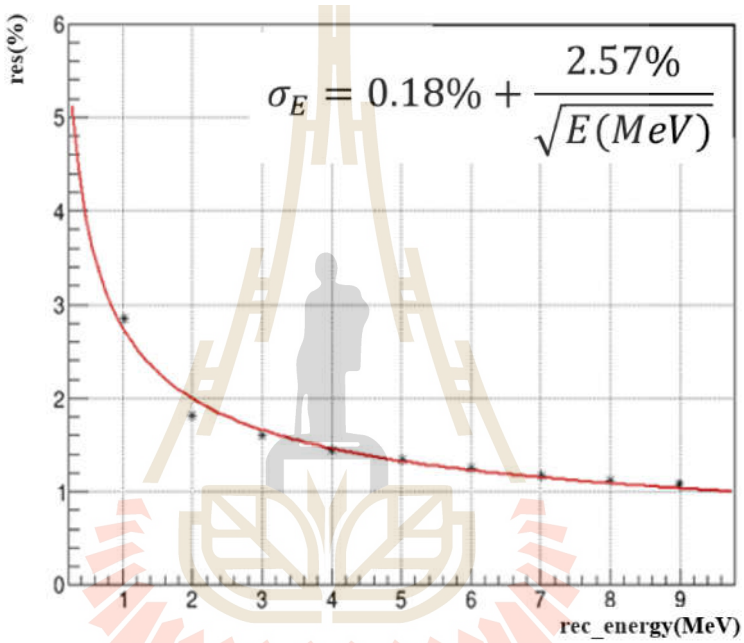

Figure 1.5 Detector energy resolution from simulation.

These PMTs are extremely light sensitive detectors in the ultraviolet, visible, and near-infrared ranges of the electromagnetic spectrum. The PMT is very sensitive to external magnetic fields. The efficiency of the PMTs is above 90% when the external magnetic field is lower than $10\mu T$ as shown in Figure 1.6. The earth magnetic field (EMF) passing through the PMTs without any shielding would largely reduce the efficiency of the PMTs (Aiello et al., 2012).

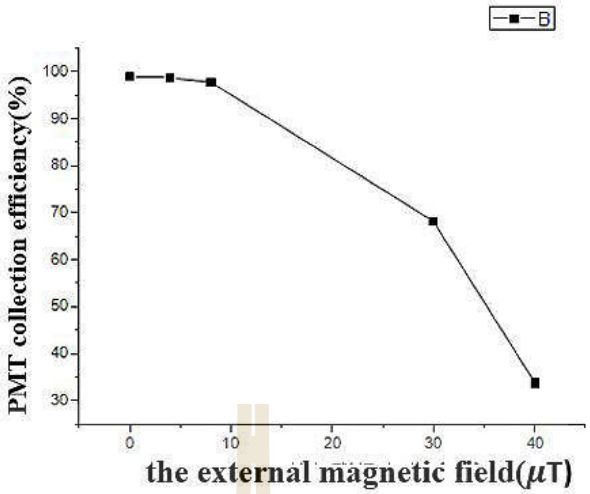

Figure 1.6 The PMTs collection efficiency in the external magnetic field.

At this moment there plenty experiment groups try to detect the neutrino oscillation such as Daya Bay, Super-Kamiokande, Sudbury and others. They used photomultiplier tubes (PMTs) to indirectly detect neutrinos. PMTs in the water pool or the Veto-PMT of JUNO can detect the light, the so-called Cherenkov light. Cherenkov light in JUNO experiment is happened by muon from the background (Adam et al., 2015) . While anti-neutrino from the reactors interacted with a proton, via invert beta decay (IBD), they caused for the birth of a neutron and a positron. The reaction of IBD can be seen as the below reaction

$$\bar{\nu}_e + p \longrightarrow n + e^+. \tag{1.8}$$

After the interaction of antineutrino and proton, a positron annihilates with an electron and produce a pair of γ-rays. The delayed signal is coming from neutron captured by Gadolinium (Gd) or hydrogen then releases UV-vis photons or γ-rays during a ground state of Gd or hydrogen from an excited state as in Figure 1.7. The UV-vis photons or γ-rays transfer energies to electrons via Compton scattering. The electrons in Compton scattering deposit energy in

the liquid scintillator via ionization. The deposit energy is afterwards altered into scintillation photons in the LAB. Then, the PPO and the bis-MSB will transfer the wavelengths of scintillation photons to longer wavelength to escape self-absorption by the LAB which the reference wavelength is generally chosen by PMTs as 430 nanometers (Zhou et al., 2015; Xing-Chen et al., 2015).

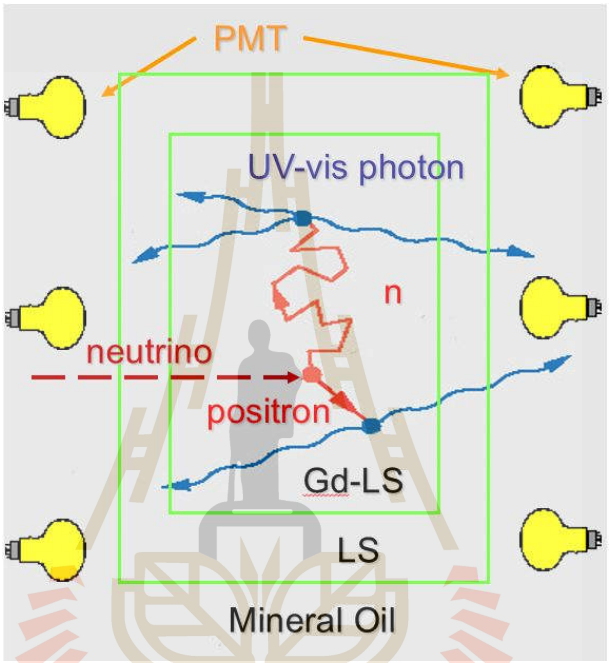

Figure 1.7 Interactions in Liquid scintillator.

Photons from the liquid scintillator are converted to photoelectrons through photoelectric effect on the thin alkali metal layer covering at The inside front surface of the glass of a PMT, The so-called photocathode. A high-speed photoelectron strike the first dynode surface with a high positive voltage and emits several secondary electrons from it to the nearest neighbor dynode. This process is repeated at each of the following dynodes to produce more secondary electrons. Finally, the electrons are obtained at the anode as an electrical signal (Cherry et al., 2012). PMTs are light extremely sensitive detector. But our world has the earth magnetic field (EMF) that can defect the direction of photoelectrons and the

secondary electrons(Aiello et al., 2012; Malace et al., 2013). The effect of EMF on the secondary electrons leads to strong effect for detection efficiency as shown in Figure 1.9, the results shows the detection efficiency between unshield (Left) and shield (Riht) EMF.

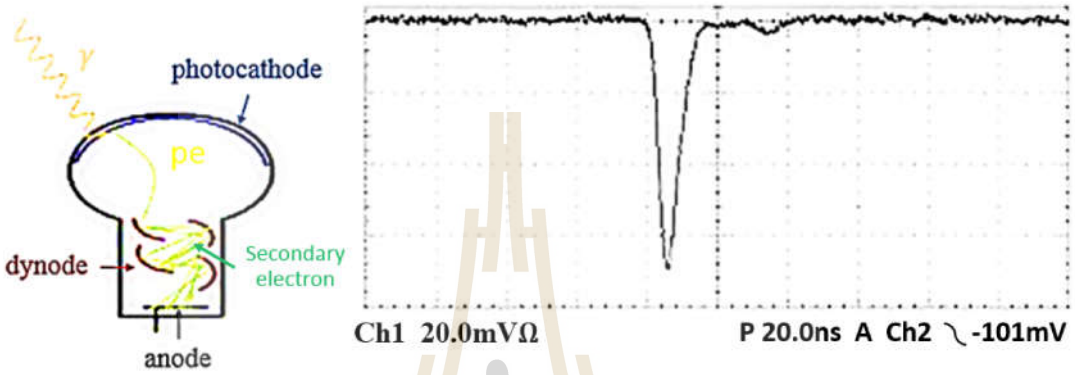

Figure 1.8 Scheme of the processes for detecting a photon by a PMT (left). An example of a single photon signal from a PMT as the peak of the amplitude at a time in the vertical axis (Kulikovskiy, 2014) (right).

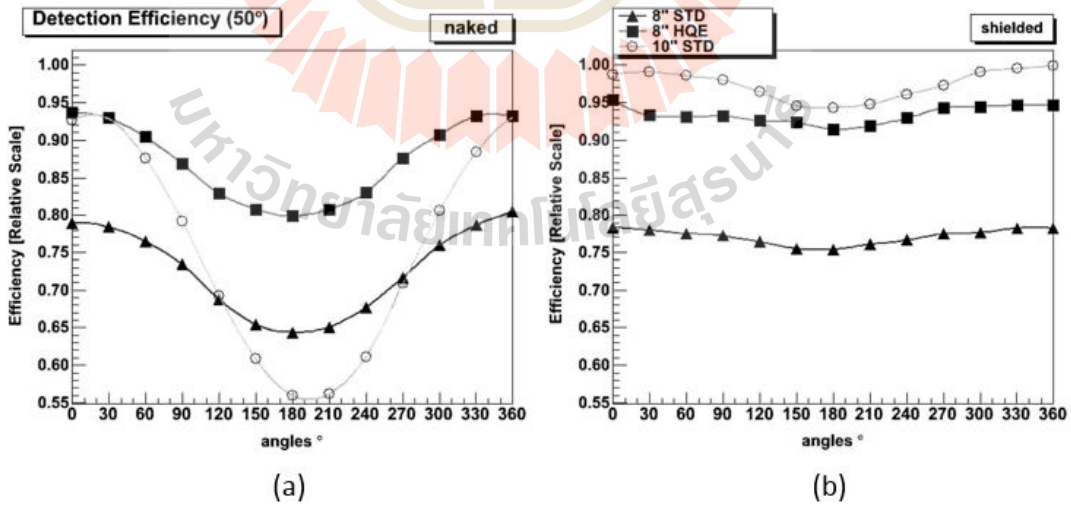

Figure 1.9 Detection efficiency between unshield(a) and shielded(b) EMF in rotating their model (Aiello et al., 2012).

In order to decrease the effect of pe trajectory from EMF, JUNO has been planing to use the DC coils for shielding EMF in PMTs region in order to reduce the effect of the Earth's geomagnetic field at Jiangmen. A strength of the geomagnetic field at Jiangmen is approximately 0.5 Gauss or 50μT. The DC in the coils will create a circumferential magnetic field around of the coils. The EMF Coils shielding for JUNO aims to get the residual intensity to less than 10 % (Lu and Baussan, 2016). So, the purpose of this thesis is design coils model for JUNO to get the residual intensity lower than 10 % in the CD PMT regions and 15 % in the veto PMT regions.

CHAPTER II

THE BIOT-SAVART'S LAW WITH NUMERICAL INTEGRATION AND OPTIMIZATION

The Maxwell's equations is well known and plays a crucial role in electromagnetism. These equations describe an effect from electric and magnetic fields and are also applied for making navigational, communication, scientific tools, and so on. Some of these tools are made for cancellation of the EMF in the world. The cancellation of the EMF needs to make an equipment that can generate a homogeneous magnetic field. The Helmholtz coils is a popular tool for creating uniform magnetic field and also applied for calibration magnetic fields sensors (Jr. and Hoff, 2001; Park et al., 2008; Park et al., 2010). However, the inside region of the Helmholtz coils have only homogeneity field in a small region (Bell and Marino, 1989). In large region of homogeneity field can be generated by adding the coils which are going to be discussed later.

2.1 The geomagnetic field

The world has a magnetic field at every location and a different in each location. A giant magnet source has various sources. These source are materials or compositions in itself. The electric current can produce a magnetic field as known. Therefore, the rapid electric currents in the liquid outer core inside the Earth is stronger source than can generate the magnetic field. The liquid outer

core consists mainly of metallic iron (Maus et al., 2010). In addition, the unstable electric currents in the core causes the different fields on the Earth's surface and the change of the magnetic field. The hypothesis of the main magnetic field is that the EMF is a pure potential field. Thus, it can be written as the negative gradient of a scalar potential

$$\vec{B}_m = -\vec{\nabla} V, \tag{2.1}$$

where V is a potential at the Earth's surface. A potential at the Earth's surface is a sum of the internal and external potentials of the Earth. Nevertheless, the external potential is too small compared with the internal potential. A potential can therefore be expanded in terms of spherical harmonics as

$$V = a \sum_{n=1}^{\inf} \sum_{m=0}^{n} \left(\frac{a}{r}\right)^{n+1} P_n^m(\cos\theta)[g_n^m \cos m\lambda + h_n^m \sin m\lambda], \tag{2.2}$$

where a is a geomagnetic reference radius, λ, θ and r are the longitude, latitude and radius in a spherical geocentric reference frame, $P_n^m(\cos\theta)$ are the normalized associated Legendre functions, and g_n^m and h_n^m are spherical harmonic coefficients or Gauss coefficients of degree n and order m which are called the main field coefficients. The components of the magnetic field vector are determined as

$$X' = \frac{1}{r}\frac{\partial V}{\partial \theta}, \tag{2.3}$$

$$Y' = -\frac{1}{r\sin\theta}\frac{\partial V}{\partial \lambda}, \tag{2.4}$$

$$Z' = \frac{\partial V}{\partial r}. \tag{2.5}$$

Actually, The above formulas are not the true fields at the Earth's surface, The components X', Y', and Z' must be oriented along the rotational axis of the Earth. In magnetic measurements at the Earth's surface, satellites made the coefficients g_n^m and h_n^m, and the main magnetic field from many practical mission and scientific work around the world. Those knowledges led to publish International Geomagnetic Reference Field (IGRF) by the International Association of Geomagnetism and Aeronomy (IAGA). Magnetic elements from IAGA consists of the true north X, east Y, and vertical Z components of the geomagnetic field, the horizontal intensity H, the total intensity F, the magnetic declination D, and the magnetic inclination I. The last four elements defined as

$$H = \sqrt{X^2 + Y^2}, \tag{2.6}$$

$$F = \sqrt{H^2 + Z^2}, \tag{2.7}$$

$$D = \arctan(\frac{Y}{X}), \tag{2.8}$$

$$I = \arctan(\frac{Z}{H}). \tag{2.9}$$

Since the JUNO is located in Jiangmen which have the latitude 22.5787 degrees north and the longitude 113.0819 degrees east. Magnetic elements from the IGRF's computation in 20 years (1997-2017) gave the north component $X \approx 37.9152\mu T$, the east component $Y \approx -1.4430\mu T$, the vertical components $Z \approx 24.4728\mu T$, the horizontal intensity $H \approx 37.9431\mu T$, the total intensity $F \approx 45.1527\mu T$, the magnetic declination $D \approx -2.1804$ degrees, and magnetic inclination $I \approx 32.8198$ degrees. Magnetic declination and magnetic inclination changed -0.0591 degrees per year and 0.1340 degrees per year, respectively. The altered angles in each

year is significant to be considered for the EMF shielding by using the DC coils. Because the different magnetic inclination causes for varying the EMF.

2.2 Biot-Savart's law

The Biot-Savart's law defined mathematically in term of a curent-carrying I along a wire as

$$\vec{B} = \frac{\mu_0}{4\pi} \int \frac{I d\vec{l} \times \vec{r}}{|\vec{r}|^3}, \tag{2.10}$$

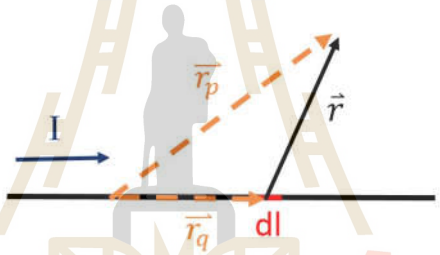

Figure 2.1 A straight wire carrying a current I.

where μ_0 is a permeability of air, I is a steady current, $\vec{l}$ is the length of the wire in the direction of a steady current and $\vec{r}$ is a displacement vector from a wire to the field point (Griffiths, 2013). The Eq. 2.10 uses to calculate a magnetic field from a source on a field point. This dissertation will solve a magnetic field from the straight lines in the Cartesian coordinate which start from a cross product of a length of a straight line in the direction of a steady current $\vec{l}$ and a displacement vector from a source (x_q,y_q,z_q) to a field (x_p,y_p,z_p) points $\vec{r}$ by

$$d\vec{l} = dx_q\hat{i} + dy_q\hat{j} + dz_q\hat{k}, \tag{2.11}$$

and

$$\vec{r} = (x_p - x_q)\hat{i} + (y_p - y_q)\hat{j} + (z_p - z_q)\hat{k}. \tag{2.12}$$

So, the magnetic fields from a straight line in cartesian coordinate are given by

$$B_x = \frac{\mu_0 I}{4\pi}\left[\int \frac{z_p - z_q}{\sqrt{(x_p - x_q)^2 + (y_p - y_q)^2 + (z_p - z_q)^2}^3} dy_q - \int \frac{y_p - y_q}{\sqrt{(x_p - x_q)^2 + (y_p - y_q)^2 + (z_p - z_q)^2}^3} dz_q\right], \tag{2.13}$$

$$B_y = \frac{\mu_0 I}{4\pi}\left[\int \frac{x_p - x_q}{\sqrt{(x_p - x_q)^2 + (y_p - y_q)^2 + (z_p - z_q)^2}^3} dz_q - \int \frac{z_p - z_q}{\sqrt{(x_p - x_q)^2 + (y_p - y_q)^2 + (z_p - z_q)^2}^3} dx_q\right], \tag{2.14}$$

$$B_z = \frac{\mu_0 I}{4\pi}\left[\int \frac{y_p - y_q}{\sqrt{(x_p - x_q)^2 + (y_p - y_q)^2 + (z_p - z_q)^2}^3} dx_q - \int \frac{x_p - x_q}{\sqrt{(x_p - x_q)^2 + (y_p - y_q)^2 + (z_p - z_q)^2}^3} dy_q\right]. \tag{2.15}$$

Above equations are a magnetic field on x, y, and z axes, respectively. Finally, these equations are taken for simulating coils model. The computational simulation will be used to study the coils model. A modeling for Biot-Savart's law has to use the numerical integration which is approximately by using numerical techniques (Krommer and Ueberhuber, 1998).

2.3 Numerical integration

In general, numerical integration is employed to calculate approximately the definite integral of function $f(x)$ in the region [a,b],

$$S = \int_a^b f(x)dx. \tag{2.16}$$

The region [a,b] can be separated to be points of lattice spacing by an even number n with an interval h, it can be defined as,

$$n = \frac{b-a}{h}. \tag{2.17}$$

The reason for dividing the interval [a,b] into points of lattice spacing is to estimate exactly the value from integrating of f(x) between -h and h. An approxiamte integration can be written as a linear combination of integrals in each of these intervals (Koonin and Meredith, 1990). The simplest approximation is acquired from estimating f(x) in the region $[x_i, x_{i+1}]$ linearly. This approximation can be described in the summation with $i = 0, 1, ..., N-1$ as,

$$S = \frac{h}{2}\sum_{i=0}^{N-1}(f_i + f_{i+1}) + O(h^2), \tag{2.18}$$

where $O(h^2)$ is the error in this interpolation of f(x). The Eq. 2.18 is the well-known trapezoidal rule. A better approximation can be obtained by working on two lattice spacings together and applying the lagrange interpolation to f(x) in the region $[x_{i-1}, x_{i+1}]$,

$$\begin{aligned} f(x) = {} & \frac{(x-x_i)(x-x_{i+1})}{(x_{i-1}-x_i)(x_{i-1}-x_{i+1})}f_{i-1} + \frac{(x-x_{i-1})(x-x_{i+1})}{(x_i-x_{i-1})(x_i-x_{i+1})}f_i \\ & + \frac{(x-x_{i-1})(x-x_i)}{(x_{i+1}-x_{i-1})(x_{i+1}-x_i)}f_{i+1} + O(h^3). \end{aligned} \tag{2.19}$$

The approximate result from taking integration with the Eq. 2.19 can give

a higher accuracy which can be described as,

$$S = \frac{h}{3} \sum_{j=0}^{N/2-1} (f_{2j} + 4f_{2j+1} + f_{2j+2}) + O(h^4), \tag{2.20}$$

the so-called Simpson's rule (Pang, 2006). As shown in the Eq. 2.20, Simpson's rule will obtain precisely to two orders higher than the trapezoidd rule. The most direct numerical integration technique uses the Newton-Cotes formulas or quadrature formulas which approximate a tabulated function to find the fitting polynomials. Nevertheless, the Newton-Cotes formulas has a lot of techniques. But, the best numerical method of integration is Gaussian quadrature method (Weisstein, 2018). Gaussian quadrature provides a greatly accurate and efficient algorithm for integrating functions. Because special functions are used for this integral technique that automatically minimize the feasible errors since the deviation of estimated functions from the data. Nevertheless, Gaussian quadrature uses orthogonal polynomials to solve an integral. But, the orthogonal polynomial is chosen that is the Legendre polynomials. The Gaussian quadrature of the Legendre polynomials is called Gauss-Legendre quadrature which is the simplest integration problem. The Legendre polynomials is the polynomials on the interval [-1,1]. However, a range of a definite integral is not only the interval [-1,1], it must be changed into any interval. Fortunately, the Eq. A.2 can help us to convert the range of the Legendre polynomial as the interval [a,b]. In addition, the advantage of Gauss-Legendre quadrature is that it has less iteration for computation than the trapezoidal and the Simpson's rules. So, the magnetic fields of the Eq. 2.13 to 2.15 are determined by Gauss-Legendre quadrature. For more details about Gauss-Legendre quadrature, appendix A has provided already.

2.4 Numerical Optimization

Macroscopic physical problems are cleared up by computational method which is widely known in areas of physics. But, those problems are solved impressively by numerical optimization. Numerical optimization need to identify firstly some objective. The objective relies on definite characteristics of the system, called variables or unknowns. The goal of optimization is to determine values of the unknowns that optimize the objective (Nocedal and Wright, 2006). The electric currents can be optimized by solving linear systems $Ax = b$. A is a rectangular matrix of dimension m-by-n while x is an eigen vector with n elements, and $b \in \Re^m$. This linear system is called LSMR. An iterative method LSMR is proposed for solving linear systems and least-square problems. LSMR consists of three problems, that is, unsymmetric equations, linear least-square (LS), and regularized least-square. This dissertation intends to compute a solution x in LS problem (Fong and Saunders, 2010). An element of x is sometimes a negative value, some of problem do not desire a negative value. Hence, this is the reason for presenting LS problem. LS method can deal with appearing a negative value of an element of x. Before discussing LS problem, LS problem need to be explained first. In LS problems, the objective function f has the following special form:

$$f(x) = \frac{1}{2}\sum_{j=1}^{m} r_j^2(x), \tag{2.21}$$

where each r_j is a smooth function from $\Re^n$ to $\Re$ or a residual vector, and this case assumes that $m \geqslant n$. The derivatives of f(x) can be written in terms of the Jacobian of r, which is the m $\times$ n matrix of first partial derivatives

$$\nabla f(x) = J(x)^T r(x), \tag{2.22}$$

the Jacobian of r is defined as

$$J(x) = \left[\frac{\partial r_j}{\partial x_i}\right]_{\substack{j=1,2,\ldots,m \\ i=1,2,\ldots,n}}. \tag{2.23}$$

A residual vector $(r_j(x))$ is a difference between model predictions $(\phi(x;t_j))$ and observed values (y_j), $r_j(x) = \phi(x;t_j) - y_j$. The general form of the model predictions is

$$\phi(x;\alpha) = \sum_{i=1}^{n} J_i(\alpha)x_i. \tag{2.24}$$

Therefore, the residuals can be described as

$$r_j(x) = \left(\sum_{i=1}^{n} J_i(t_j)x_i\right) - y_j, \;\; j = 1, 2, \ldots, m \tag{2.25}$$

or in matrix terms

$$r = \begin{pmatrix} J_1(t_1) & J_2(t_1) & \cdots & J_n(t_1) \\ J_1(t_2) & J_2(t_2) & \cdots & J_n(t_2) \\ \vdots & \vdots & \ddots & \vdots \\ J_1(t_m) & J_2(t_m) & \cdots & J_n(t_m) \end{pmatrix} \begin{pmatrix} x_1 \\ x_2 \\ \vdots \\ x_n \end{pmatrix} = \begin{pmatrix} y_1 \\ y_2 \\ \vdots \\ y_m \end{pmatrix} = Jx - y. \tag{2.26}$$

The point of least-square technique is to compute x for minimizing the gradient of objective function f(x) (Nocedal and Wright, 2006). Each element of Jacobian matrix is constant for linear least-square technique. The linear least-squares technique provides a solution from seeking the best fitting straight line through a set of points and finds a solution with bounds on the unknowns, the so-called the constrained linear least squares technique. Actually, the constrained linear least squares technique has a lot of methods. This dissertation is going to use bounded-variable least squares method (BVLS) in anyway. This method is linear least squares technique with the upper (ub) and lower (lb) bounds on the un-

knowns. BVLS has been claimed to be numerically stable and is comparable with a standard simplex method of a linear programming problem. BVLS algorithm was encountered to be computationally more efficient with run times up to 10 times shorter. BVLS uses an active set strategy which is similar to non-negative least squares method (NNLS) of Lawson and Hanson (Lawson et al., 1995). But, NNLS is not necessary to be maintained two active sets for variables. Two active sets mean lower and upper bounds of the unknowns. BVLS solves the problem as the following condition,

$$\min_{lb \leq x \leq ub} 0.5 \cdot \|\mathbf{Ax} - \mathbf{b}\|^2, \tag{2.27}$$

where A is an m by n matrix, b is a target vector with m elements, and x is the unknown vector with n variables. So, BVLS is used to optimize the n currents in the coils shielding problem.

CHAPTER III

COILS DESIGN FOR THE MAGNETIC FIELD SIMULATION

3.1 The Generating coil

In the magnetic calculation, a coil with a large distance from a center of a coil and a small thickness can be assumed as a line that conveys a current. A sequence for inputting the source points (x_q,y_q,z_q) on a coil are important to specify the vector of a current and the resultant vector of the magnetic induction from a current-carrying coil. For example, if the coil in Figure 3.1 desires to induce the magnetic field along the z-axis, the geometry defined as the following equations,

$$x_q = R\cos(\theta),$$

$$y_q = R\sin(\theta),$$

$$z_q = h.$$

Where R and h are a radius and a relative distance from the origin to the center of the coil, respectively. If the theta θ starts from zero to 2π, the current must flow in counterclockwise direction. For more details, the geometric program shows in appendix C. The results of the geometric program gives arrays of three points in the Cartesian coordinates.

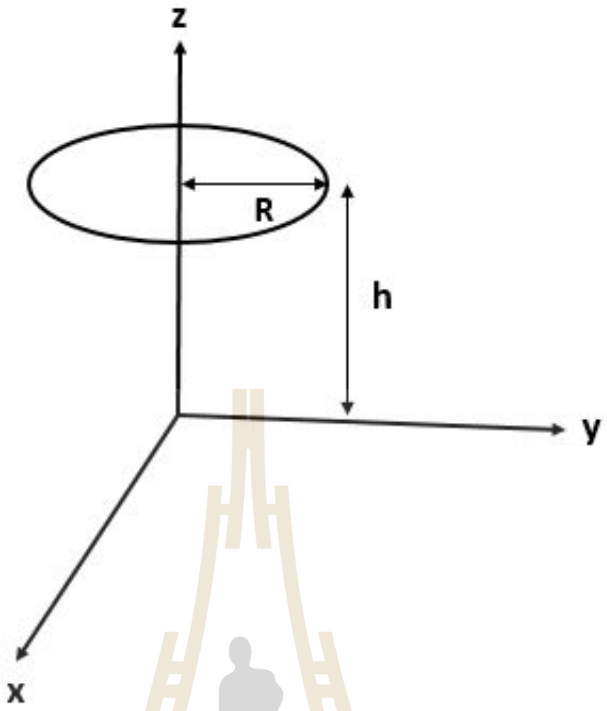

Figure 3.1 Circular coil with the radius (R) and the relative distance from the origin to the center (h) of the coil.

3.2 The Currents optimization

The optimal design can help to extrapolate an amount of the devices for an experiment. Because It can simulate the physical problems in obtaining the suitable results. Therefore, the optimal design currents carrying filament is too useful to save the cost of electrical devices. However, the optimal design for reaching the proper currents primarily uses the least squares method. In this dissertation, the currents is found by using the linear constrained least squares method, the so-called the bounded-variable least squares (BVLS). The unknowns of BVLS is sought by using the `lsq_linear` function of a Python-based ecosystem of open-source software, named Scipy (Jones et al., 2001). The package requires a m-by-n design

matrix A and a target vector b with m elements, the variables or unknowns with n elements is confined by the minimum and maximum variables. In this physical problem, each coefficient of the matrix A is from evaluating The Biot-Savart law in the Cartesian coordinates by setting a current I equal 1. The magnetic fields in the Cartesian coordinates is determined numerically in the form of a straight line as the Eq. 2.13 to 2.15 The matrix A can be written in a matrix form as

$$A = \begin{pmatrix} Bx_{11} & Bx_{12} & \cdots & Bx_{1n} \\ By_{11} & By_{12} & \cdots & By_{1n} \\ Bz_{11} & Bz_{12} & \cdots & Bz_{1n} \\ Bx_{21} & Bx_{22} & \cdots & Bx_{2n} \\ By_{21} & By_{22} & \cdots & By_{2n} \\ Bz_{21} & Bz_{22} & \cdots & Bz_{2n} \\ \vdots & \vdots & \ddots & \vdots \\ Bx_{m1} & Bx_{m2} & \cdots & Bx_{mn} \\ By_{m1} & By_{m2} & \cdots & By_{mn} \\ Bz_{m1} & Bz_{m2} & \cdots & Bz_{mn} \end{pmatrix}, \tag{3.1}$$

where, Bx_{mn}, By_{mn}, and Bz_{mn} are the summation of magnetic induction in the Cartesian coordinates of the m^{th} field point and the n^{th} coil. A coefficients of a target vector b are the EMF in the Cartesian coordinates which is defined as

$$b = \begin{pmatrix} EMFx_1 \\ EMFy_1 \\ EMFz_1 \\ EMFx_2 \\ EMFy_2 \\ EMFz_2 \\ \vdots \\ EMFx_m \\ EMFy_m \\ EMFz_m \end{pmatrix}, \tag{3.2}$$

where $EMFx_m$, $EMFy_m$, and $EMFz_m$ are the EMF in the x-axis, the y-axis, and the z-axis of the m^{th} field point, respectively. Finally, The program gives the currents of n coils in an array after The matrix A and matrix b were input in the `lsq_linear` function.

3.3 The Magnetic field calculation

The optimized currents needs to use for computing and analyzing the magnetic induction on an interesting region. However, if some of the results do not converge to the appropriate solutions, that problem is necessary to check in the following way,

- The important thing for numerical integration is a number of points that are used to compute an integration. Because numerical integration is a summing up the results of every point on a filament, the points must sometimes be added a quantity.

- It might be possible that the function for evaluating the magnetic induction is wrong. In this case, the analytic equations can help in checking the results. For instance, the magnetic field equations for any field points in the Cartesian coordinates of a circular loop can be written in the elliptic integral form ($E(k^2)$, $K(k^2)$) as

$$B_x = \frac{Cxz}{2\alpha^2\beta\rho^2}[\left(a^2 + r^2\right) E(k^2) - a^2 K(k^2)] \tag{3.3}$$

$$B_y = \frac{Cyz}{2\alpha^2\beta\rho^2}[\left(a^2 + r^2\right) E(k^2) - a^2 K(k^2)] \tag{3.4}$$

$$B_z = \frac{C}{2\alpha^2\beta}[\left(a^2 - r^2\right) E(k^2) + a^2 K(k^2)], \tag{3.5}$$

where x, y, and z are the difference between a field point and a source point in the Cartesian coordinates, a is a radius of a circular loop, $\rho^2 \equiv x^2+y^2$, $r^2 \equiv x^2+y^2+z^2$, $\alpha^2 \equiv a^2 + r^2 - 2a\rho$, $\beta^2 \equiv a^2 + r^2 + 2a\rho$, $k^2 \equiv 1 - \alpha^2/\beta^2$, and $C \equiv \mu_0 I/\pi$ (Simpson et al., 2001). Elliptic integrals can be seen as generalizations of the inverse trigonometric functions. In this case, the elliptic integral uses the complete elliptic integral of the first kind $E(k^2)$ and the complete elliptic integral of the second kind $K(k^2)$ functions of Scipy package (Abramowitz and Stegun, 1964). If the results is consistent with the results from equation 3.6 to equation 3.8, the coil system is rearranged to the new location to get better results.

3.4 The coils model characterization

The effect of EMF to PMTS is a big problem for accurately measuring the neutrino signals. Thus, the PMTS has to be prevented from the geomagnetic field which is able to be done by using the coils. Since the EMF has three dimensions, the compensation coils must therefore induce the magnetic fields for canceling the EMF in three dimensions. The agreed parameter for selecting the coils model is the residual intensity R. From Figure 1.6, The residual intensity should not be over 10 % (Lu et al., 2017). However, The intensity below 15 % is acceptable for shielding on the Veto-PMT region. The residual intensity defined as

$$R = \frac{\sqrt{(B_x - EMF_x)^2 + (B_y - EMF_y)^2 + (B_z - EMF_z)^2}}{EMF} \times 100\%, \qquad (3.6)$$

where EMF, EMF_x, EMF_y, and EMF_z are the resultant , the northern, the eastern, and the vertical of EMF, respectively. The EMF in the Cartesian coordinates is subtracted by the magnetic inductions from the coils (B_x,B_y,B_z).

CHAPTER IV

RESULTS AND DISCUSSIONS

4.1 Two sets of coils

4.1.1 Introduction

In present, the JUNO experiment has the model as shown in Figure 1.4. The first model for JUNO is similar to the model in Figure 1.4. But, the first model consists of PMTs on the wall and bottom parts which is displayed in Figure 4.1. As mentioned in the first chapter, the EMF has very strong effect on the PMTs. So, the coils shielding is chosen to cancel the EMF which is 37.988 μT or 0.37988 Gauss in the north, 0.01505 Gauss in the east, and 0.23772 Gauss in the vertical directions as shown in Figure 4.2. Since the geomagnetic field in the eastern is too small comparing with the others directions. For convenient installation, Institute of High Energy Physics (IHEP) proposed two sets of the circular coils model to cancel out the EMF in the north and the vertical directions. This dissertation is going to indicate the residual intensities on the spherical surfaces of diameter 39, 39.5, 40, 41, 41.5, and 41.8 meters by choosing about 16,000 points on its. The spherical surfaces cover the area of outside and inside the CD-PMT and the Veto-PMT.

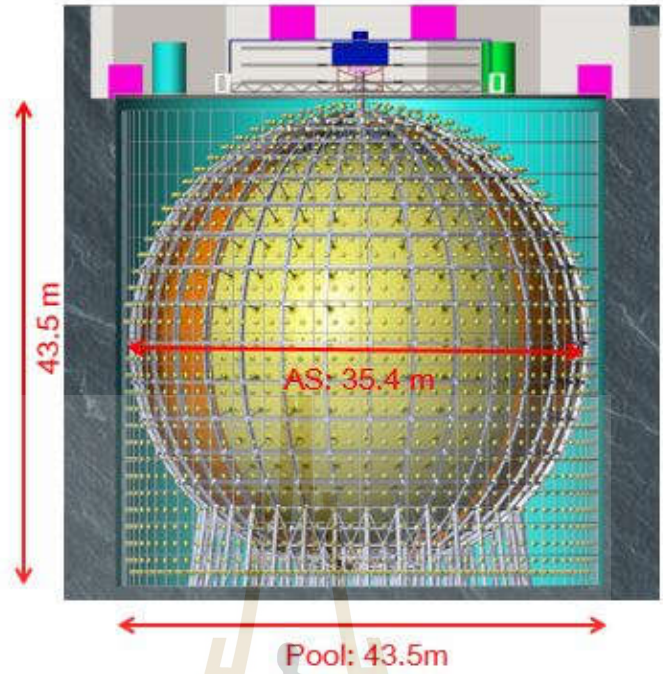

Figure 4.1 The first JUNO experimental model.

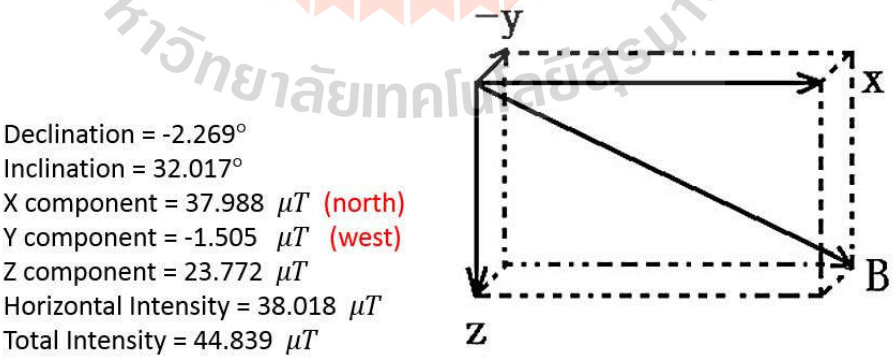

Figure 4.2 The geomagnetic field in Jiangmen.

4.1.2 The cylindrical and the spherical models

This model is proposed by Institute of High Energy Physics (IHEP) which composes of the 26 circular coils in cylindrical shape and the 30 circular coils in spherical shape. The 26 coils induces magnetic fields in the vertical direction while the 30 coils is used to shield the EMF in the north direction. As introduced in the third chapter, these coils models are decided by the maximum residual intensity. The maximum residual intensity will be calculated in order to use to compare the EMF shielding coils models. Fortunately, the magnetic fields in the Cartesian coordinates for a circular coil has the analytical form as shown in the Eq. 3.3 to 3.5. The magnetic fields in a numerical method is computed by summing up in each direction of the generated magnetic fields from small straight lines that connected to be a circle. In this calculation, a circular coil produces a magnetic field from 1000 of small straight lines.

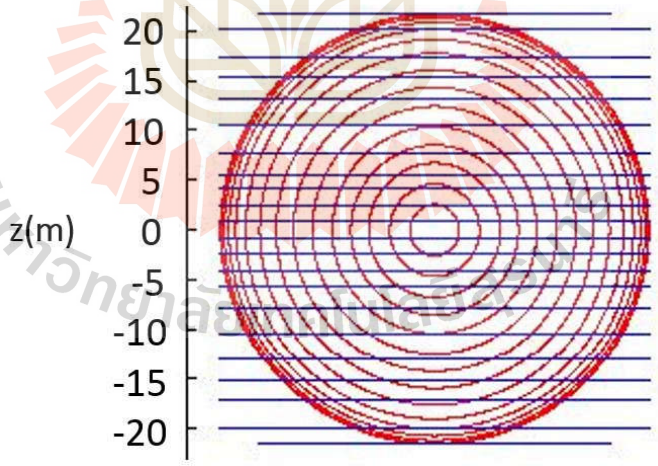

Figure 4.3 The cylindrical model plus the spherical model.

Before the results is indicated, Table 4.1 and Table 4.2 are respectively the parameters of the cylindrical and the spherical models. The parameters consists of the label number of coils (Coil), the radius of coils (R), and the relative distance

from the origin to a center of each coil (H), and the currents (I). The currents I of these model were optimized by using BVLS method and linear regression calculate the ampere per turn. A turn of the cylindrical model has 11.755 amperes while a turn of the spherical model has 10.322 amperes.

Table 4.1 The parameters of the cylindrical model.

Coil	R(m)	H(m)	I(A)	Coil	R(m)	H(m)	I(A)
1,26	6.50	±21.65	23.51	8,19	21.65	±10.47	58.77
2,25	13.00	±21.65	58.77	9,18	21.65	±7.80	58.77
3,24	17.90	±21.65	70.53	10,17	21.65	±5.62	35.26
4,23	21.65	±20.10	141.06	11,16	21.65	±4.10	35.26
5,22	21.65	±17.30	58.77	12,15	21.65	±2.44	35.26
6,21	21.65	±15.25	47.02	13,14	21.65	±0.83	35.26
7,20	21.65	±13.100	58.77	-	-	-	-

Table 4.2 The parameters of the spherical model.

Coil	R(m)	H(m)	I(A)	Coil	R(m)	H(m)	I(A)
1,30	2.59	±21.50	10.32	9,22	17.69	±12.49	103.22
2,29	4.62	±21.26	20.64	10,21	19.10	±10.20	103.22
3,28	6.74	±20.56	30.96	11,20	20.10	±8.05	92.89
4,27	8.53	±19.90	30.96	12,19	20.80	±6.01	92.89
5,26	10.39	±19.00	51.61	13,18	21.26	±4.06	82.57
6,25	12.40	±17.75	61.93	14,17	21.52	±2.38	72.25
7,24	14.30	±16.26	72.25	15,16	21.64	±0.79	72.25
8,23	16.02	±14.56	82.57	-	-	-	-

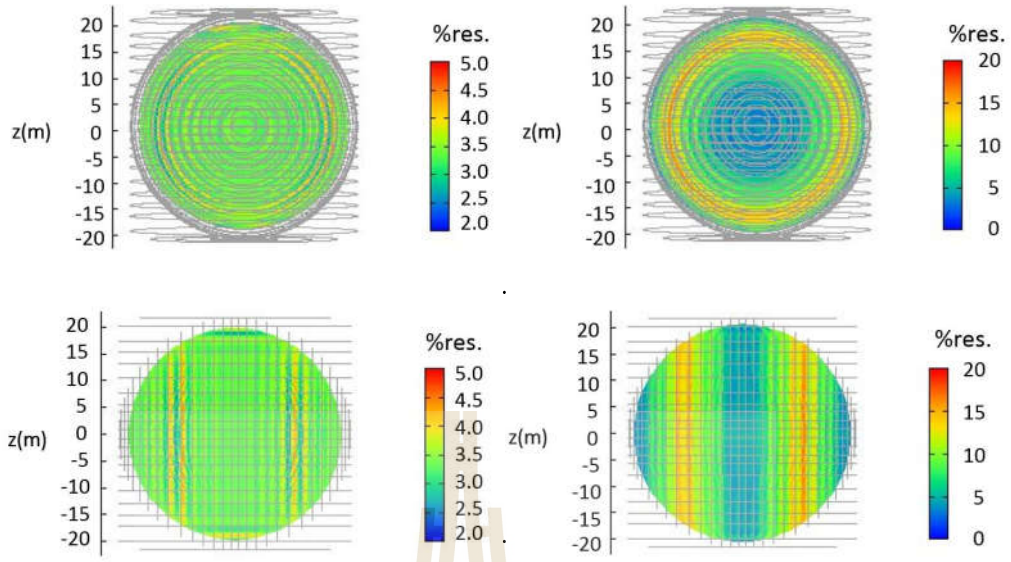

Figure 4.4 Spherical surface plot of the residual intensities on the CD-PMT (left panel) and the Veto-PMT (right panel).

Now, the maximum residual intensities in PMT regions of this model are shown and compared with the analytical results as Table 4.3. So, the results indicated that the results from numerical technique (Simulation) is consistent with the analytical results. However, the maximum residual intensities is more than 15 % on the Veto-PMT and less than 10 % on the CD-PMT. Moreover, the spherical surface plot on the CD-PMT and the Veto-PMT are displayed in Figure 4.4. The result of the spherical surface plot does clearly describe the strongest and the weakest regions of a residual intensity. The plots present a front and a side views which has the highest intensity region is nearby the coils with the current 122.2 ampere or the highest current. Finally, the histogram plot of the residual intensities on the CD-PMT and Veto-PMT is perspective which can tell the average and the maximum residual intensity.

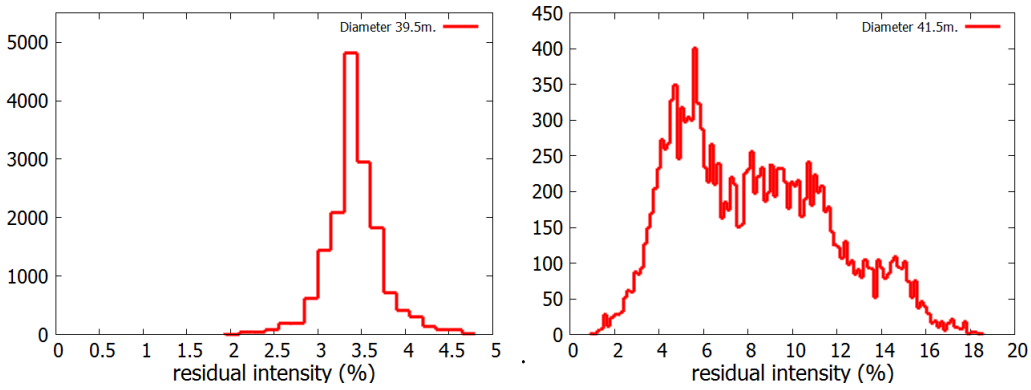

Figure 4.5 Histogram plot of the residual intensities on the CD-PMT (left figure) and the Veto-PMT (right figure).

Table 4.3 The maximum residual intensity of the spherical surfaces of the cylindrical model plus the spherical model.

Diameters(m)	Maximum resiudal intensity	
	Simulation(%)	Analytic(%)
39.00	4.13	4.36
39.50	4.71	4.96
40.00	5.82	5.99
41.00	11.57	11.63
41.50	18.51	18.82
41.80	25.59	26.46

4.1.3 The cylindrical and the rectangular coils models

This model still uses the cylindrical model as the previous model and is likewise the idea of IHEP. But, the spherical model is replaced by the rectangular model. The currents passes through the rectangular coils as the model in Figure 4.6. With the same amount of coils of the spherical model, the widths (W) of the rectangular model has the interval [10.560,43.300] meters while the heights (2z) of coils are the same as shown in Table 4.4. For enlargement of the second set of coils, it may get better results. Finally, Table 4.5 shows that most of the maximum residual intensities over 15 % and do not accord to assumption.

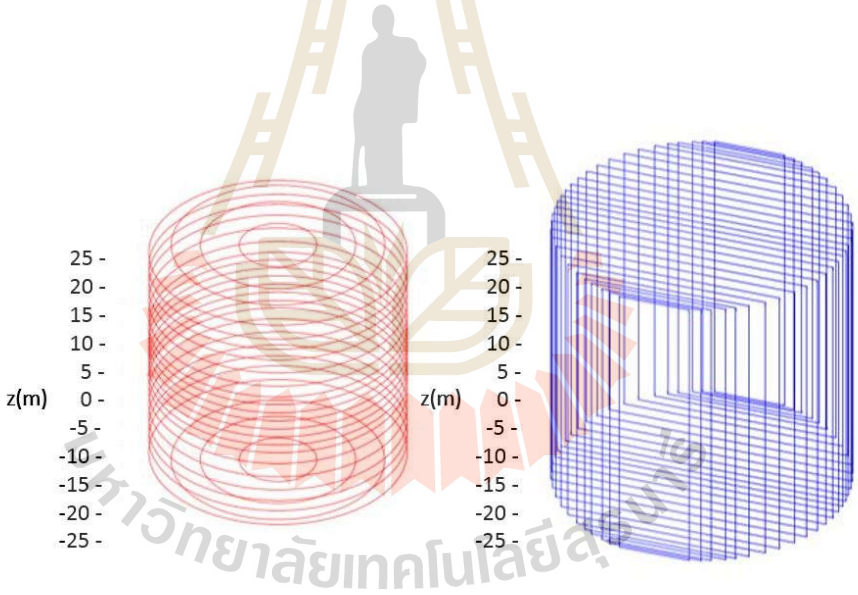

Figure 4.6 The cylindrical model plus the rectangular model.

Table 4.4 The parameters of the rectangular model.

Coil	W(m)	2z(m)	H(m)	I(A)	Coil	W(m)	2z(m)	H(m)	I(A)
1,30	10.56	43.32	±21.00	21.60	9,22	36.32	43.32	±11.80	108.00
2,29	13.94	43.32	±20.50	21.60	10,21	38.62	43.32	±9.80	86.40
3,28	16.60	43.32	±20.00	64.80	11,20	40.42	43.32	±7.80	97.20
4,27	20.40	43.32	±19.10	64.80	12,19	41.72	43.32	±5.83	86.40
5,26	23.00	43.32	±18.35	43.20	13,18	42.60	43.32	±3.95	86.40
6,25	26.18	43.32	±17.25	75.60	14,17	43.08	43.32	±2.24	75.60
7,24	30.04	43.32	±15.60	86.40	15,16	43.30	43.32	±0.70	64.80
8,23	33.22	43.32	±13.90	108.00	-	-	-	-	-

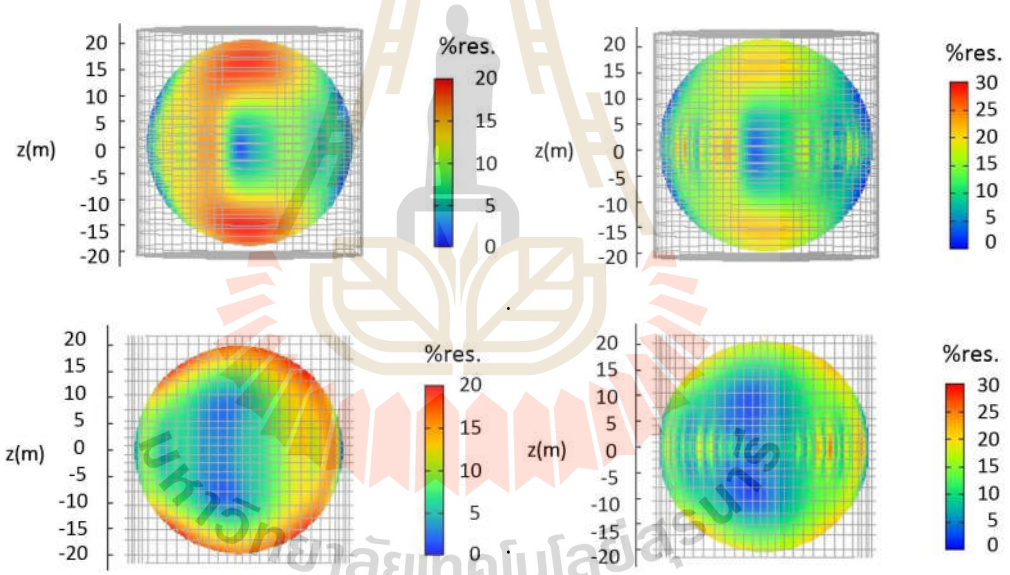

Figure 4.7 Spherical surface plot of the residual intensities on the CD-PMT (left panel) and the Veto-PMT (right panel) of the cylindrical model plus the rectangular model.

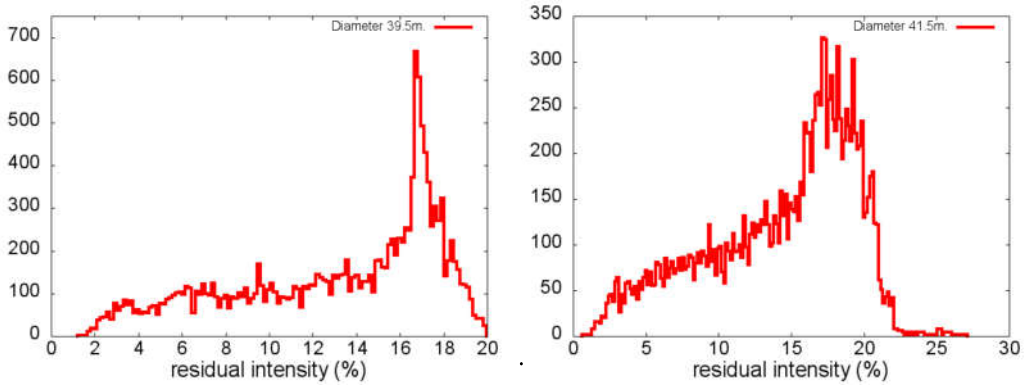

Figure 4.8 Histogram plot of the residual intensities on the CD-PMT (left figure) and the Veto-PMT (right figure) of the cylindrical model plus the rectangular model.

Table 4.5 The maximum residual intensity of the spherical surfaces of the cylindrical model plus the rectangular model.

Diameters(m)	Maximum residual intensity(%)
39.00	19.39
39.50	19.88
40.00	20.39
41.00	21.95
41.50	26.98
41.80	34.17

4.1.4 The cylindrical and the gate shape coils models

This model is proposed by Suranaree University of Technology (SUT). The gate shape coils model is shown as in Figure 4.12. The gate shape is designed to shield the PMTs on the bottom region and supported by the truss of CD. The parameters are the same as the rectangular model. But the upper part of the coils are substituted by the half circles with radius as half of the widths of the rectangles on the lower part of the coils. The calculation of the maximum residual intensity of the results of the previous model give the similar results of the previous model and emphasizes that the coils including a long straight line is unable to give an accepted residual intensity. The maximum residual intensities of the CD-PMT are above 10 % and the Veto-PMT over 15 % as shown in Table 4.7. Finally, this model is able to prevent the EMF on the upper half region of the CD-PMT, the maximum residual intensity of the CD-PMT on the upper half region equal to 7.36 % and the maximum residual intensity of the Veto-PMT on the upper half region equal to 18.16 %.

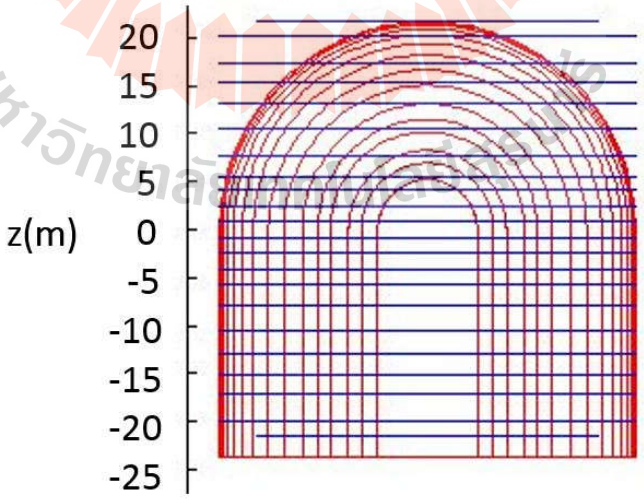

Figure 4.9 The cylindrical model plus the gate shape model.

Table 4.6 The parameters of the gate shape model.

Coil	R(m)	W(m)	z(m)	H(m)	I(A)	Coil	R(m)	W(m)	z(m)	H(m)	I(A)
1,30	5.28	10.56	23.66	±21.00	12.56	9,22	18.16	36.32	23.66	±11.80	110.06
2,29	6.97	13.94	23.66	±20.50	26.73	10,21	19.31	38.62	23.66	±9.80	98.45
3,28	8.30	16.60	23.66	±20.00	30.49	11,20	20.21	40.42	23.66	±7.80	92.77
4,27	10.20	20.40	23.66	±19.10	36.90	12,19	20.86	41.72	23.66	±5.83	90.95
5,26	11.50	23.00	23.66	±18.35	51.33	13,18	21.30	42.60	23.66	±3.95	80.65
6,25	13.09	26.18	23.66	±17.25	67.97	14,17	21.54	43.08	23.66	±2.24	70.45
7,24	15.02	30.04	23.66	±15.60	68.50	15,16	21.65	43.30	23.66	±0.70	70.04
8,23	16.61	33.22	23.66	±13.90	97.40	-	-	-	-	-	-

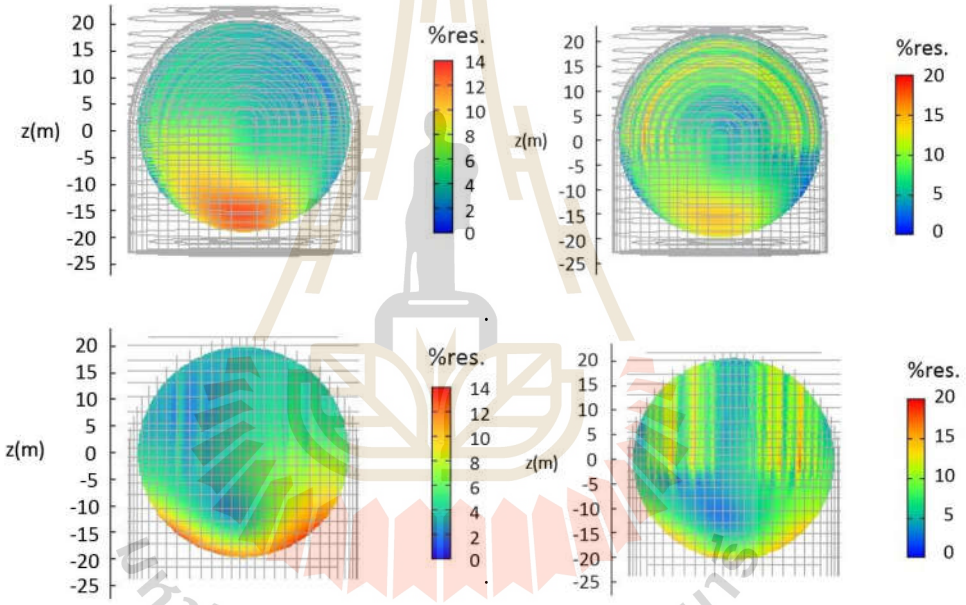

Figure 4.10 Spherical surface plot of the residual intensities on the CD-PMT (left panel) and the Veto-PMT (right panel) of the cylindrical model plus the gate model.

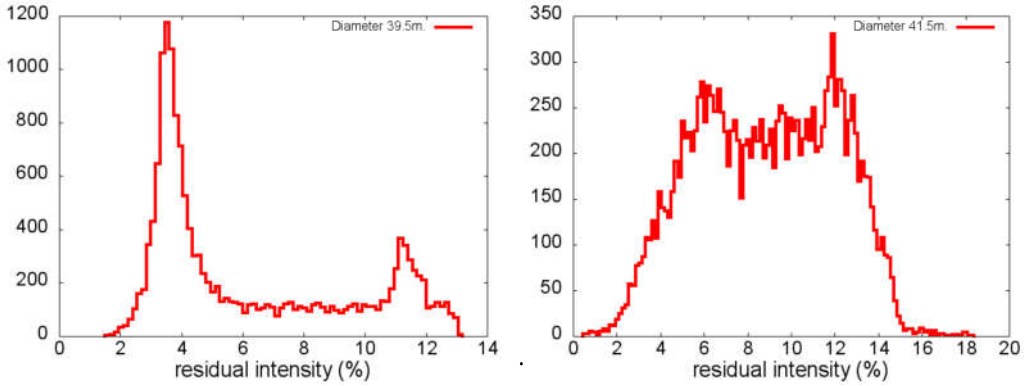

Figure 4.11 Histogram plot of the residual intensities on the CD-PMT (left figure) and the Veto-PMT (right figure) of the cylindrical model plus the gate model.

Table 4.7 The maximum residual intensity of the spherical surfaces of the cylindrical model plus the gate shape model.

Diameters(m)	Maximum residual intensity(%)
39.00	12.69
39.50	13.08
40.00	13.48
41.00	14.35
41.50	18.16
41.80	24.68

4.1.5 The cylindrical and the octagon coils models

From IHEP's simulation, they found that a small part on a coil overlaps with the supporting truss. This problem led to take into account an octagon coil which this model was proposed by SUT and National Astronomical Research Institute of Thailand (NARIT). This model still uses the cylindrical model and replaces the spherical model by the octagon model that a shape of coils is an octagon as shown in Figure 4.12. The octagon coils has a width Y equal to a length Z which appear in Table 4.8. The maximum residual intensities are a little bit worse than the cylindrical model plus the spherical model as shown in Table 4.9. Nevertheless, the octagon coils shields the EMF on the CD-PMT region as same as the circular coils.

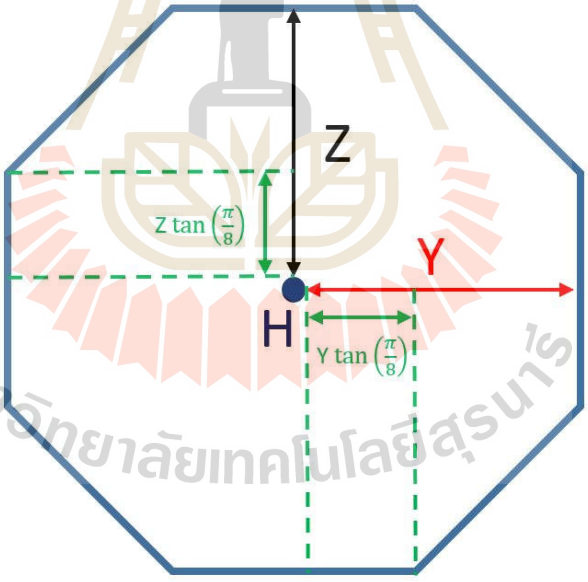

Figure 4.12 An octagon coil and it parameters.

Table 4.8 The parameters of the octagon model.

Coil	Y(m)	Z(m)	H(m)	I(A)	Coil	Y(m)	Z(m)	H(m)	I(A)
1,30	2.59	2.59	±21.50	10.32	9,22	17.69	17.69	±12.49	102.55
2,29	4.62	4.62	±21.26	23.54	10,21	19.10	19.10	±10.20	103.32
3,28	6.74	6.74	±20.56	28.63	11,20	20.10	20.10	±8.05	94.71
4,27	8.53	8.53	±19.90	34.22	12,19	20.80	20.80	±6.01	92.72
5,26	10.39	10.39	±19.00	49.61	13,18	21.26	21.26	±4.06	83.31
6,25	12.40	12.40	±17.75	63.57	14,17	21.52	21.52	±2.38	73.02
7,24	14.30	14.30	±16.26	71.93	15,16	21.64	21.64	±0.79	73.00
8,23	16.02	16.02	±14.56	85.43	-	-	-	-	-

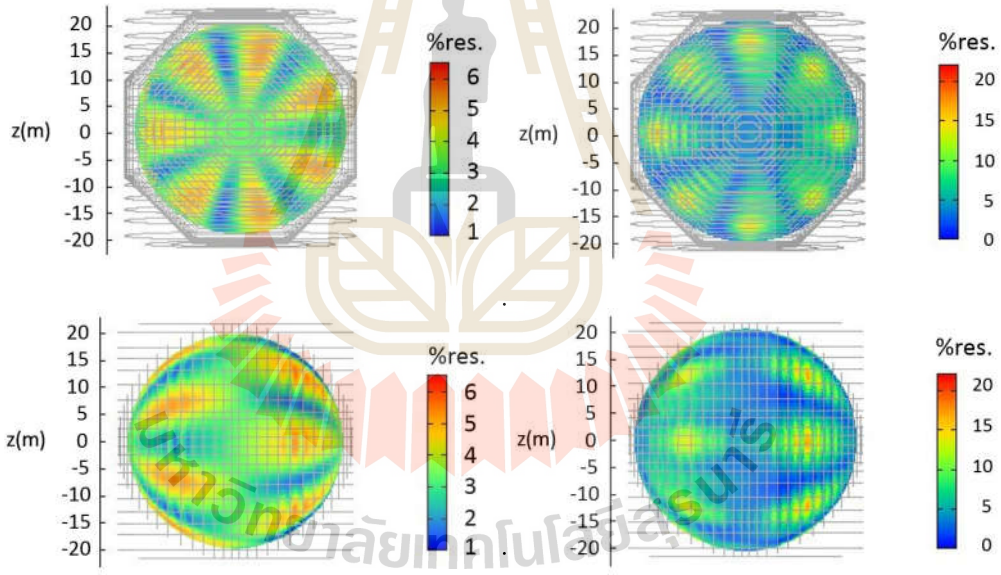

Figure 4.13 Spherical surface plot of the residual intensities on the CD-PMT (left panel) and the Veto-PMT (right panel) of the cylindrical model plus the octagon model.

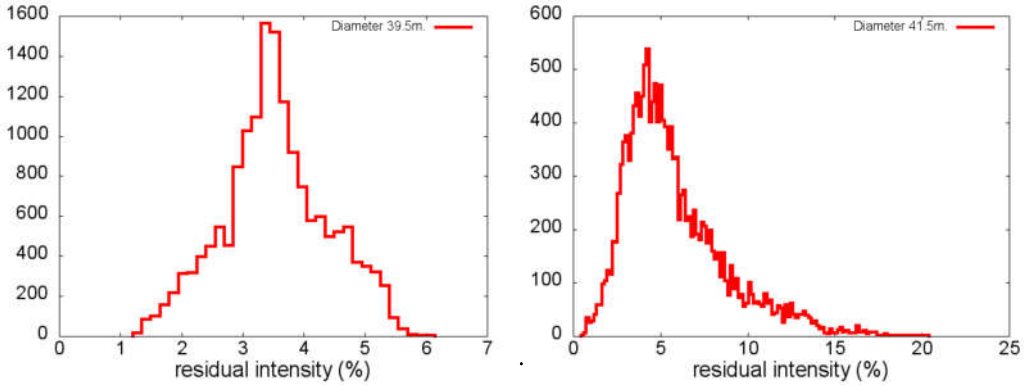

Figure 4.14 Histogram plot of the residual intensities on the CD-PMT (left figure) and the Veto-PMT (right figure) of the cylindrical model plus the octagon model.

Table 4.9 The maximum residual intensity of the spherical surfaces of the cylindrical model plus the octagon model.

Diameters(m)	Maximum residual intensity(%)
39.00	5.37
39.50	6.09
40.00	7.29
41.00	13.20
41.50	20.20
41.80	27.16

4.1.6 Summary for two sets of coils

This section concluded that the best choice of the coils shielding is the circular coils while the octagon coils is acceptable for canceling the EMF. Both the circular and the octagon coils allow the EMF to affect the efficiency of the Veto-PMT in anyway. So, if the JUNO uses the cylindrical model plus the spherical model, the JUNO needs to prevent the EMF on the Veto-PMT region by using the mu-metal. This material are surely to reach the JUNO's goal.

4.2 One set of coils

4.2.1 Introduction

The results of two sets of coils disclosed that the circular coils model is the best choice for EMF shielding. Now, JUNO is going to set up PMTs on a merely acrylic sphere as seen in Figure 1.4 and also requires to save the budget. Since coils generate the magnetic fields in the mainly normal direction to those coils. So, one set of coils which is rotated and produce the magnetic fields in the opposite direction of the EMF will be one of the solution for EMF shielding. Actually, magnetic induction to exactly the opposite direction of the EMF by coils is difficult to installation. By the way, the EMF in the west direction is very small and can be negligible. Therefore, compensation coil can induce a magnetic field in the direction aligned to about 2 degrees to the EMF direction. So, this section will study the shielding effect of one set of the circular coils model.

4.2.2 The model of 15 pairs of circular coils

This model early was proposed by SUT and Kasetsart University and was simulated firstly by IHEP. This model rotates the spherical model on the y-axis in the east direction approximately -32 degrees. However, the currents needs to be reoptimized. The results of the optimized currents are shown in Table 4.10. The currents can be folded in 12.22 ampere per turn. An arrangement of circular coils can see in Figure 4.15. It is found that a model of 15 circular coils has the achievement that the maximum residual intensity is 5.26 % in the CD-PMT (Diameter 39.5 m.) region and 21.74 % in the Veto-PMT (Diameter 41.5 m.) region. The compared results are written in Table 4.11. The maximum residual intensities of one set of circular coils is worse than the outcomes of two sets of circular coils. Eventually, the maximum residual intensity below 10 % in the CD-PMT and over 15 % in the Veto-PMT of both cases.

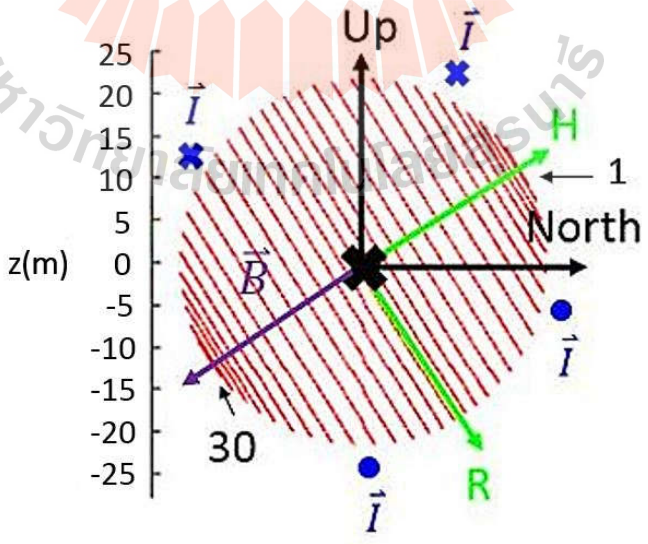

Figure 4.15 The 15 pairs of circular coils model.

Table 4.10 The parameters of the 15 pairs of circular coils model.

Coil	R(m)	H(m)	I(A)	Coil	R(m)	H(m)	I(A)
1,30	2.59	±21.50	12.22	9,22	17.69	±12.49	122.20
2,29	4.62	±21.26	24.44	10,21	19.10	±10.20	122.20
3,28	6.74	±20.56	36.66	11,20	20.10	±8.05	109.98
4,27	8.53	±19.90	36.66	12,19	20.80	±6.01	109.98
5,26	10.39	±19.00	61.10	13,18	21.26	±4.06	97.76
6,25	12.40	±17.75	73.32	14,17	21.52	±2.38	85.54
7,24	14.30	±16.26	85.54	15,16	21.64	±0.79	85.54
8,23	16.02	±14.56	97.76	-	-	-	-

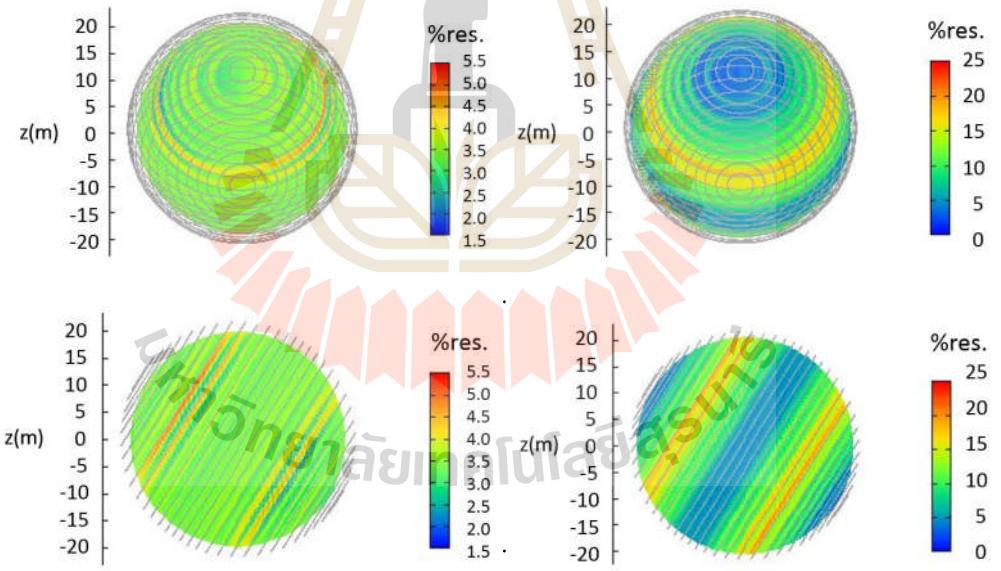

Figure 4.16 Spherical surface plot of the residual intensities on the CD-PMT (left panel) and the Veto-PMT (right panel) of the model of 15 pairs of circular coils.

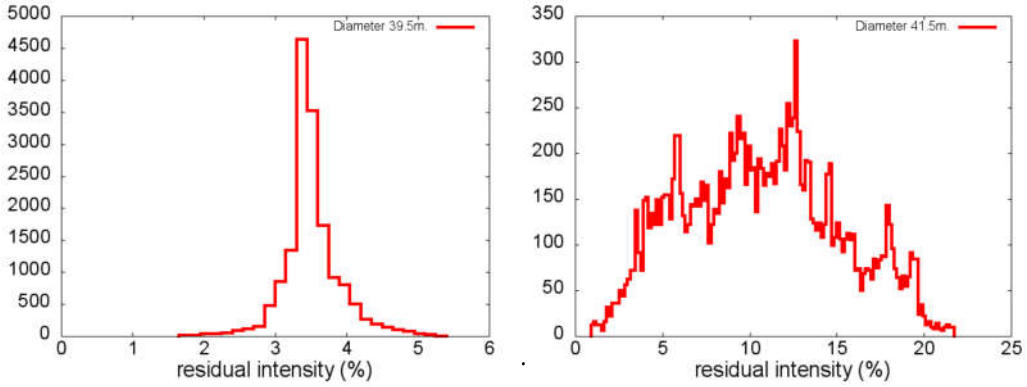

Figure 4.17 Histogram plot of the residual intensities on the CD-PMT (left figure) and the Veto-PMT (right figure) of the model of 15 pairs of circular coils.

Table 4.11 The comparison of the maximum residual intensities between one set of circular coils and two sets of circular coils.

Diameters(m)	Maximum resiudal intensity	
	One Set(%)	Two Sets(%)
39.00	4.57	4.13
39.50	5.26	4.71
40.00	6.46	5.82
41.00	13.18	11.57
41.50	21.74	18.51
41.80	30.94	25.59

4.2.3 The model of 16 pairs of circular coils with almost the same interval

This model has the same coil layouts as the 15 pairs model. But, this model is added 1 pair of circular coils and is rearranged the new position of circular coils to be almost the same interval (ΔH_{ij}) between two neighbor coils. This model has inspired from Chulalongkorn University that tried to reduce coils of the spherical

model and adapt the coils with the same interval between two neighbor coils. Then, NARIT suggested Thai-JUNO Consortium to modify the model which the coils has the interval of two neighbor coils as the same. Finally, SUT proposed the 16 pairs of circular coils with almost the same interval of two neighbor coils by using the parameters as shown in Table 4.12. An electric current is 13.181 amperes per turn. The results of this model is in agreement with the achievement that the maximum residual intensity is 5.156 % in the CD-PMT region and 13.766 % in the Veto-PMT region as shown in Table 4.13. The model of 16 pairs of circular coils (B2(16 coils)) shields the Veto PMT much better than the 15 pairs of circular coils model (B2(15 coils)) and two sets of coils or the cylindrical model plus the spherical model (B1B2) as shown in Figure 4.21 which compares the maximum residual intensity of the spherical surfaces with diameter 39.0, 39.5, 40.0, 41.0, 41.5, and 41.8 meters of three models.

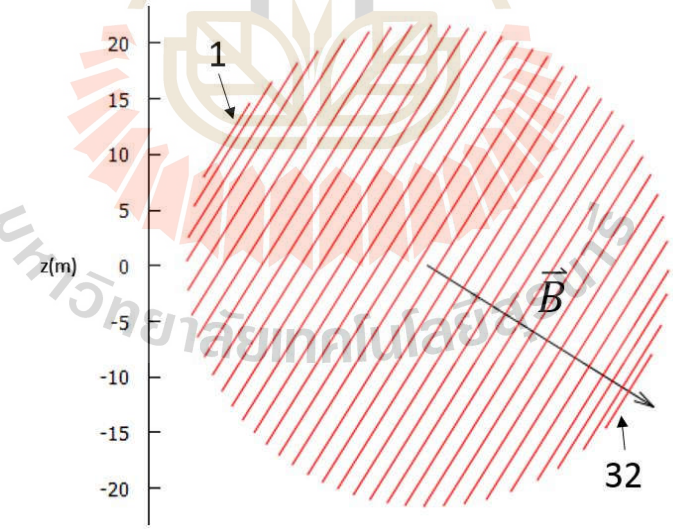

Figure 4.18 The 16 pairs of circular coils model with almost the same interval between two neighbor coils.

Table 4.12 The parameters of The 16 pairs of circular coils model with almost the same interval between two neighbor coils.

Coil	R(m)	H(m)	ΔH_{ij}(m)	I(A)	Coil	R(m)	H(m)	ΔH_{ij}(m)	I(A)
1,32	3.90	±21.30	-	26.36	9,24	18.54	±11.18	1.48	79.08
2,31	6.57	±20.63	0.67	52.72	10,23	19.36	±9.70	1.48	79.08
3,30	9.24	±19.58	1.05	52.72	11,22	20.03	±8.22	1.48	79.08
4,29	11.12	±18.58	1.00	65.90	12,21	20.57	±6.74	1.48	79.08
5,28	13.28	±17.10	1.48	79.08	13,20	21.01	±5.26	1.48	79.08
6,27	14.99	±15.62	1.48	79.08	14,19	21.32	±3.78	1.48	79.08
7,26	16.39	±14.14	1.48	79.08	15,18	21.53	±2.30	1.48	79.08
8,25	17.56	±12.66	1.48	79.08	16,17	21.63	±0.82	1.48	79.08

$\Delta H_{ij} = H_i - H_j$; $j = i + 1$; i and j stand for the i^{th} and j^{th} coils.

Table 4.13 The maximum residual intensity of the spherical surfaces of The 16 pairs of circular coils model with almost the same interval between two neighbor coils.

Diameters(m)	Maximum residual intensity(%)
39.00	4.66
39.50	5.15
40.00	5.97
41.00	9.68
41.50	13.77
41.80	18.00

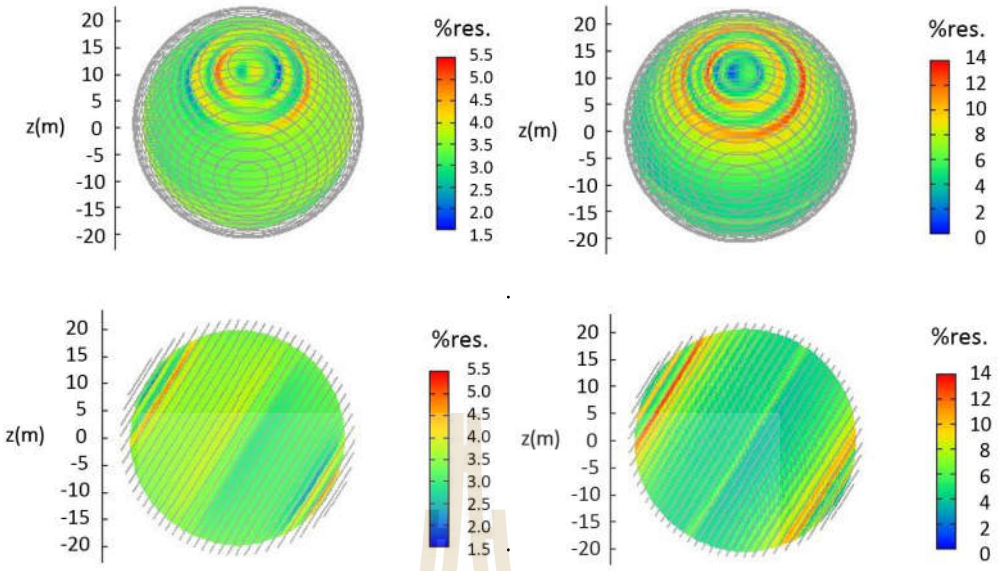

Figure 4.19 Spherical surface plot of the residual intensities on the CD-PMT (left panel) and the Veto-PMT (right panel) of The 16 pairs of circular coils model.

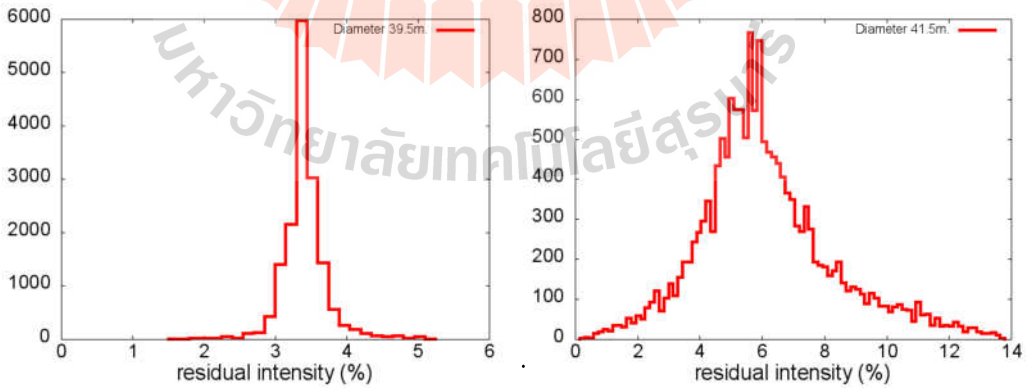

Figure 4.20 Histogram plot of the residual intensities on the CD-PMT (left figure) and the Veto-PMT (right figure) of The 16 pairs of circular coils model.

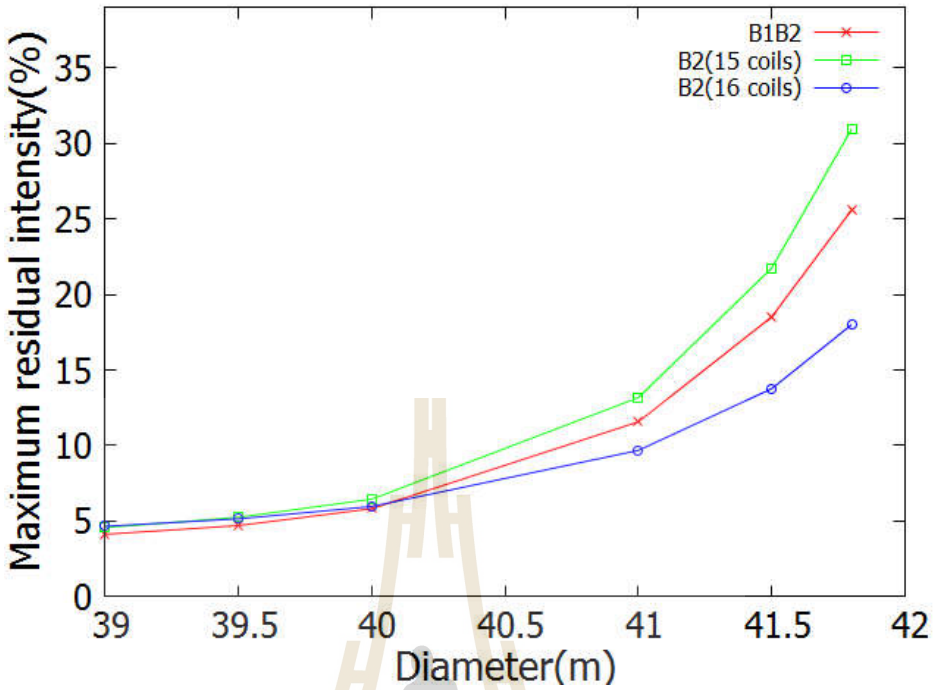

Figure 4.21 A line plot of the maximum residual intensity of the spherical surfaces (y-axis) with diameter 39.0, 39.5, 40.0, 41.0, 41.5, and 41.8 meters (x-axis) of the 16 pairs of circular coils, the 15 pairs of circular coils and the best model of two set of coils models.

4.2.4 Installation error with slightly distorted coils

In the installation process of the 16 pairs of circular coils, small bumps on the circular coils are unavoidable. This section compares the results of slightly distorted coils (half circle) with the results of perfect coils (16 pairs of circular coils) by using the parameters in Table 4.12. The possible small bump is separated into three cases as shown in Figure 4.22. These small bumps are on the coils numbered as 9, 10, 11, and 12. The maximum residual intensities of four cases are shown in Table 4.14. Finally, the results reveals that the effect of possible distortions to the coils and installation errors is negligible.

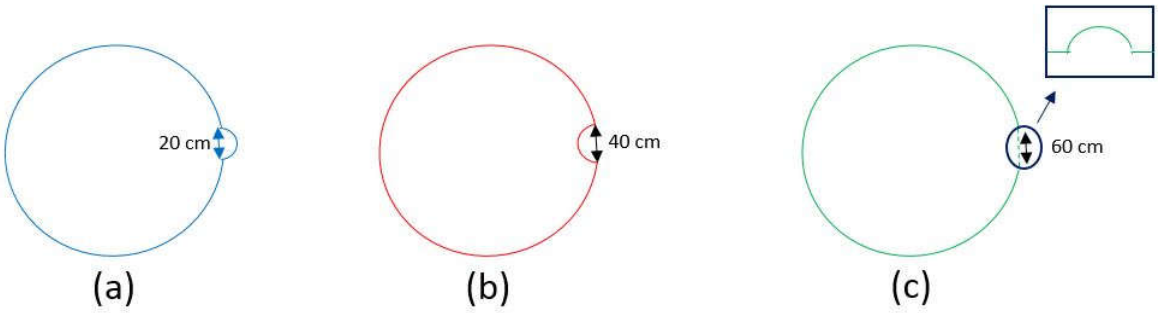

Figure 4.22 The possible small bump are shown as the pictures (a) outer half circle, (b) inner half circle, and (c) perpendicular half circle cases, respectively.

Table 4.14 The comparison of the maximum residual intensities between perfect coils and three cases of slightly distorted coils.

Diameters(m)	Maximum resiudal intensity			
	Perfect(%)	OH10(%)	IH20(%)	PH30(%)
39.00	4.66	4.81	4.80	4.76
39.50	5.15	5.19	5.19	5.19
40.00	5.97	6.03	6.03	6.02
41.00	9.68	9.76	9.76	9.76
41.50	13.77	13.95	13.95	13.94
41.80	18.00	18.25	18.25	18.25

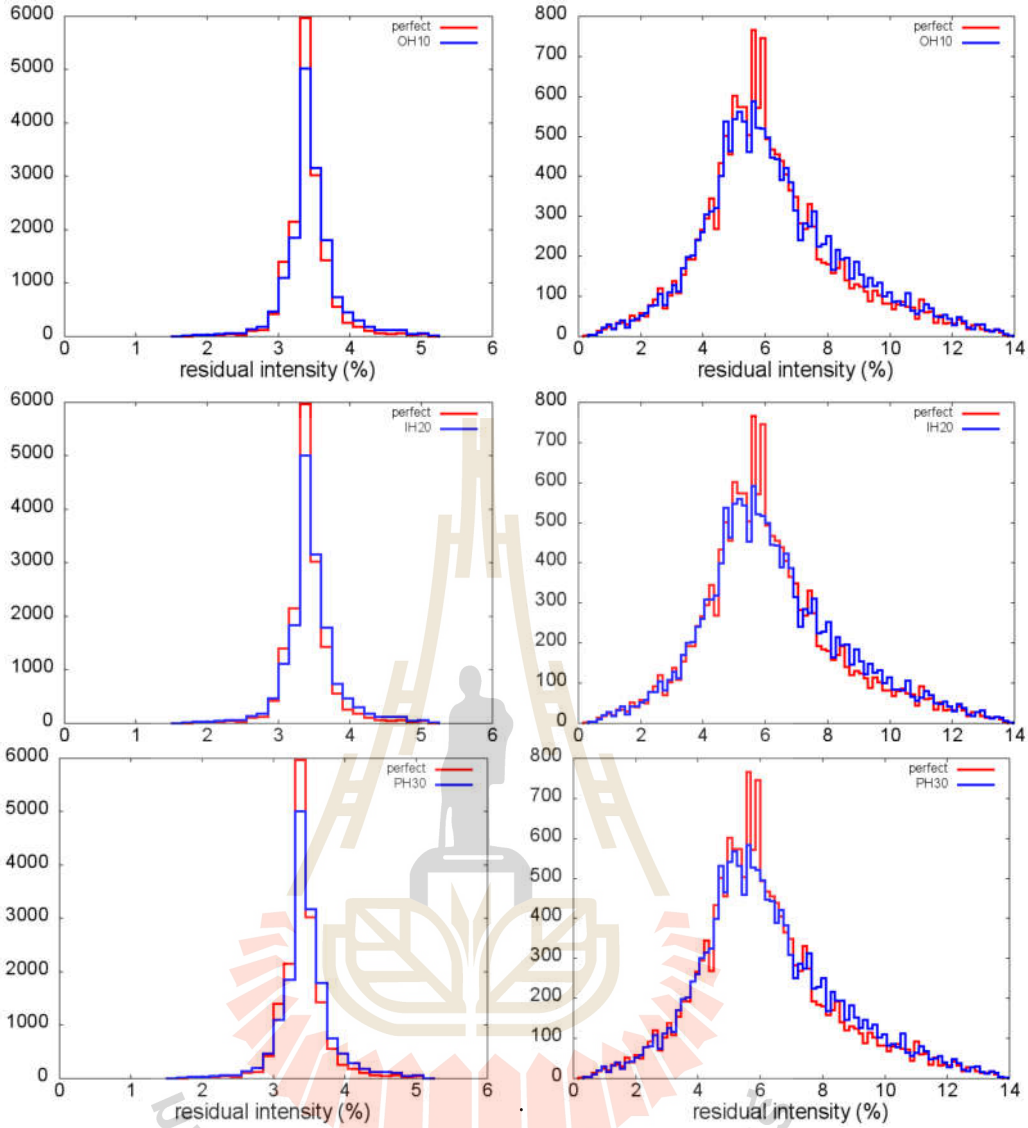

Figure 4.23 The comparison of histogram plot of the residual intensities on the CD-PMT (left panel) and the Veto-PMT (right panel) of perfect coils and three cases of slightly distorted coils.

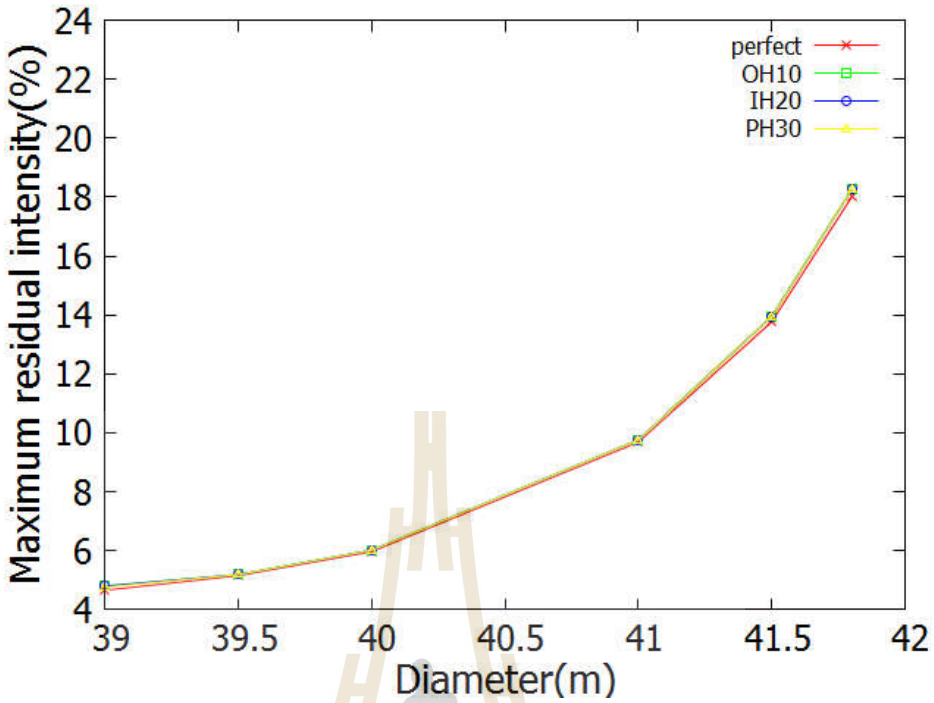

Figure 4.24 A line plot of the maximum residual intensity of the spherical surfaces (y-axis) with diameter 39.0, 39.5, 40.0, 41.0, 41.5, and 41.8 meters (x-axis) of the 16 pairs of circular coils without installation error (perfect) and three cases of slightly distorted coils.

4.2.5 Installation error with slightly displaced coils

This section compares the results of slightly displaced coils with the results of perfect coils (Perfect). These displaced coils are on the coils numbered as 8 and 9 of the model of 16 pairs of circular coils. Figure 4.24 displays four cases, there are, (1) increased the interval between two coils (a), (2) decreased the interval between two coils (b), (3) displaced two coils to its right hand side (c), (4) displaced two coils to its left hand side (d). The effect of installation error with slightly displaced coils is more influence than installation errors with small bumps. Because of the maximum residual intensities below 10 % in the CD-PMT and above 15 % as shown in Table 4.15.

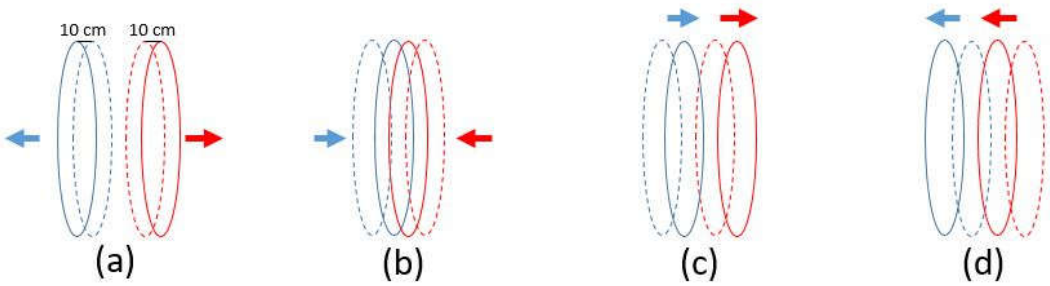

Figure 4.25 Four cases of installation error with slightly displaced coils.

Table 4.15 The comparison of the maximum residual intensities between perfect coils and four cases of slightly displaced coils.

Diameters(m)	Maximumresiudalintensity				
	Perfect(%)	a(%)	b(%)	c(%)	d(%)
39.00	4.66	4.68	4.68	4.69	4.79
39.50	5.16	5.18	5.18	5.19	5.19
40.00	5.97	6.01	6.01	6.01	6.03
41.00	9.68	9.76	9.76	9.77	9.76
41.50	13.77	13.93	13.93	13.93	13.95
41.80	18.00	18.24	18.24	18.24	18.25

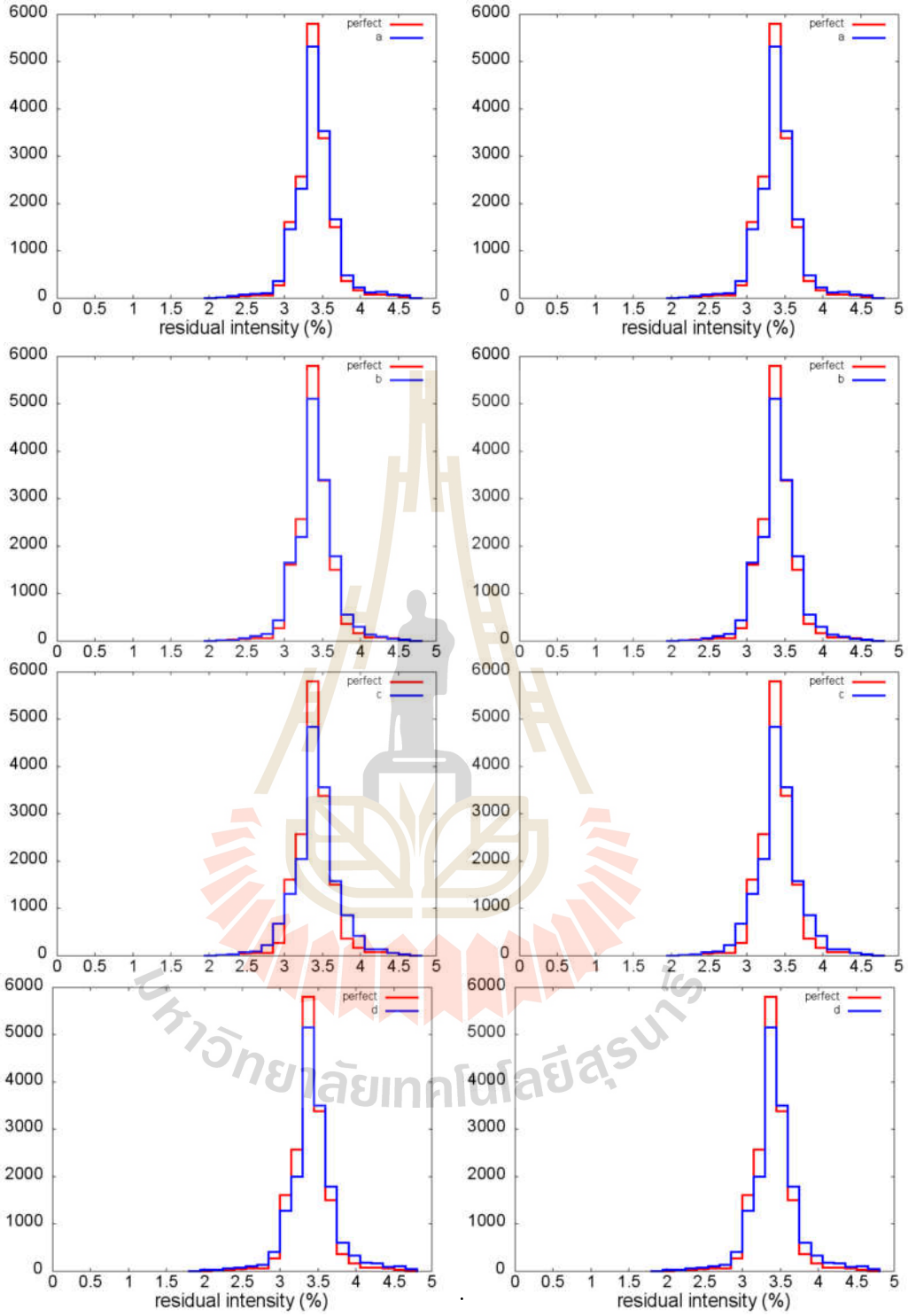

Figure 4.26 The comparison of histogram plot of the residual intensities on the CD-PMT (left figure) and the Veto-PMT (right figure) of perfect coils and four cases of slightly displaced coils.

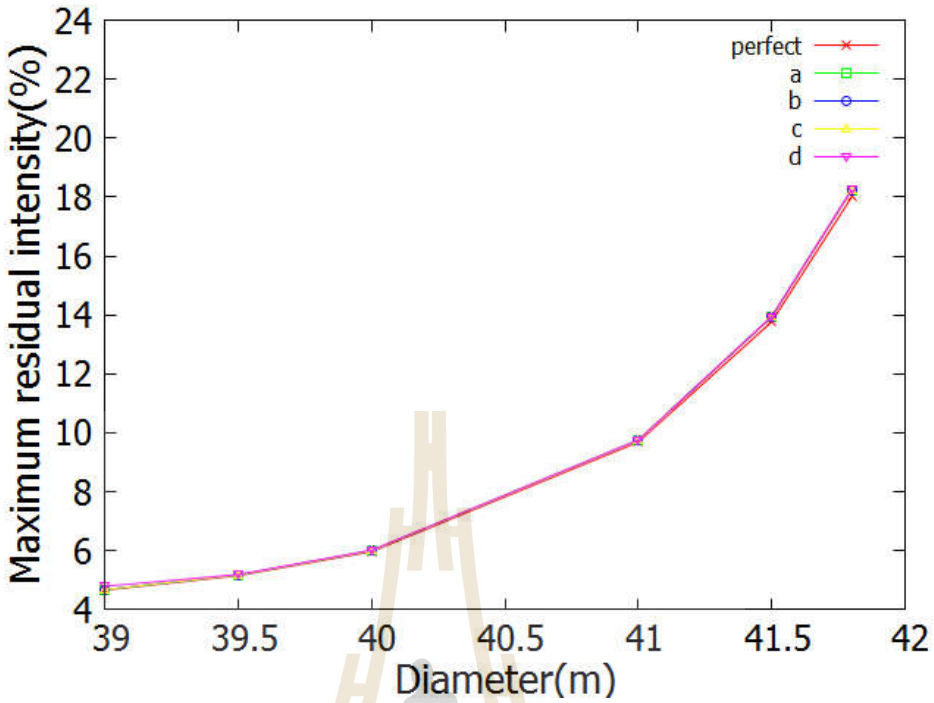

Figure 4.27 A line plot of the maximum residual intensity of the spherical surfaces (y-axis) with diameter 39.0, 39.5, 40.0, 41.0, 41.5, and 41.8 meters (x-axis) of the 16 pairs of circular coils without installation error (perfect) and four cases of slightly displaced coils.

4.2.6 Overall installation errors

In this section, the effect of possible installation error will be considered at the coils numbered as 8 and 9 of the model of 16 pairs of circular coils. We have introduced two possible installation errors previously. But the Installation error with slightly inclined coils cannot be ignored. The 8^{th} and 9^{th} coils are set up with those as shown in Figure 4.26. We separated the cases as the latest cases. It found that the influence of two inclined coils with one degree is largely to EMF shielding as shown in Table 4.16. This effect leads to reduce the efficiency of the Veto-PMT. Fortunately, the CD-PMT maintains its efficiency.

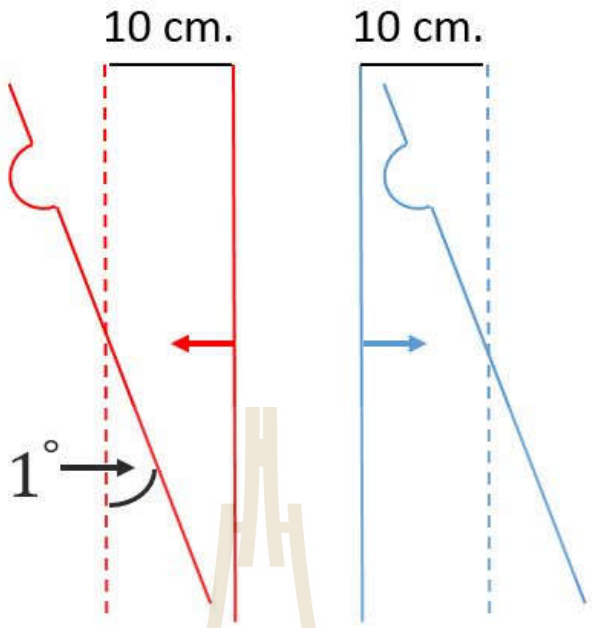

Figure 4.28 An overall installation errors coil.

Table 4.16 The comparison of the maximum residual intensities between perfect coils and four cases of overall installation errors coils.

Diameters(m)	Maximumresiudalintensity				
	Perfect(%)	a(%)	b(%)	c(%)	d(%)
39.00	4.66	6.05	6.45	6.59	6.97
39.50	5.16	6.77	7.24	7.31	7.73
40.00	5.97	7.85	8.45	8.27	8.85
41.00	9.68	12.24	13.32	12.71	13.45
41.50	13.77	17.11	18.36	17.65	18.29
41.80	18.00	22.04	22.99	22.20	22.64

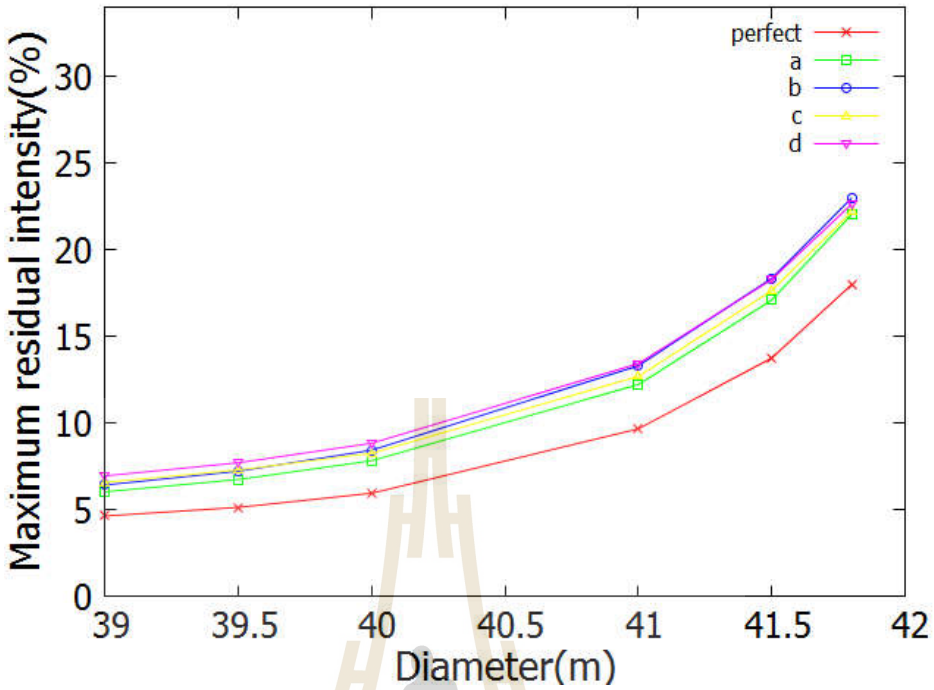

Figure 4.29 A line plot of the maximum residual intensity of the spherical surfaces (y-axis) with diameter 39.0, 39.5, 40.0, 41.0, 41.5, and 41.8 meters (x-axis) of the 16 pairs of circular coils without installation error (perfect) and four cases of overall installation errors coils.

4.2.7 EMF variation

Even though the model of 16 pairs of circular coils fulfill the JUNO requirements. However, the EMF has been changing in every year. The geomagnetic field in Jiangmen varies an inclination angle around 0.1340 degrees per year that mean an inclination angle of the EMF in Jiangmen in the next 20 years is approximately 2.68 degrees. So, EMF shielding of the model of 16 pairs of circular coils need to consider with cases of EMF varying three inclination angles, that is, 1, 2, and 3 degrees. EMF in three directions of three inclination angles are listed in Table 4.17 which rotate in a clockwise direction. The results reveals in Table 4.18 that the maximum residual intensities on the Veto-PMT above 15 % in EMF variation

with 2 and 3 degrees of inclination angles which is out of an agreement. But, the maximum residual intensities keeps up the efficiency of the PMTs.

Table 4.17 EMF variation with three inclination angles.

Direction	1°(Gauss)	2°(Gauss)	3°(Gauss)
North (X)	0.38	0.39	0.39
East (Y)	-0.01	-0.01	-0.01
Vertical (Z)	0.23	0.22	0.22

Table 4.18 The comparison of the maximum residual intensities between without the EMF variation case and three changed inclination angles cases.

Diameters(m)	Maximum resiudal intensity			
	Perfect(%)	1°(%)	2°(%)	3°(%)
39.00	4.66	5.07	6.12	7.48
39.50	5.16	5.57	6.62	7.99
40.00	5.97	6.39	7.44	8.80
41.00	9.68	10.09	11.10	12.46
41.50	13.77	14.20	15.23	16.57
41.80	18.00	18.44	19.46	20.79

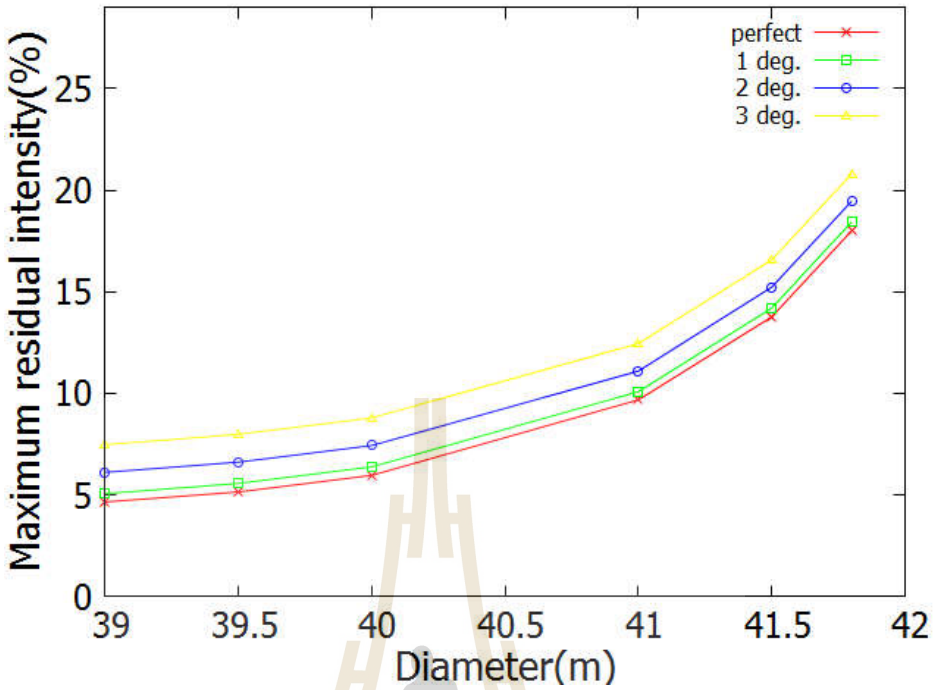

Figure 4.30 A line plot of the maximum residual intensity of the spherical surfaces (y-axis) with diameter 39.0, 39.5, 40.0, 41.0, 41.5, and 41.8 meters (x-axis) of the 16 pairs of circular coils without the EMF variation case (perfect) and three changed inclination angles cases.

4.2.8 Summary for one set of coils

We can conclude that the model of 16 pairs circular coils shields the Veto PMT much better than the 15 pairs of circular coils. Without installation errors and EMF variation, the 16 pairs of circular coils maintains the efficiency of the PMTs on both the CD-PMT and the Veto-PMT while the effect of possible distortions to the coils numbered as 9, 10, 11, and 12 and displacements to the coils nubered as 8 and 9 is negligible. But, installation error with inclined coils numbered as 8 and 9 and EMF variation largely affect to exactly determine the neutrino signals.

CHAPTER V

CONCLUSIONS

The Jiangmen Undergroud Neutrino Observatory (JUNO) is a reactor antineutrino experiment with the main purpose for determining the neutrino mass hierarchy by precisely measuring the energy spectrum of nuclear reactor electron antineutrinos. The JUNO central detector (CD) consists of approximately 18,000 20″ and 25,000 3″ PMTs while about 2,400 water Cherenkov (Veto) PMTs are installed on outer acrylic sphere. The PMTs are very sensitive to external magnetic fields, the EMF passing through the PMTs without any shielding would largely reduce the efficiency of the PMTs. In order to minimize the effect of the EMF inside the detector, JUNO has been planing to use DC coils to shield the EMF, aiming at the residual EMF less than 10 % on PMT areas.

In this work we have studied the shielding effect of various coils models. It is found that a model of 16 pairs of circular coils shields the Veto PMT much better than the model of 15 pairs of circular coils and models of two sets of coils, and also fulfill the JUNO requirements. We likewise take into account possible installation errors of the coils and the EMF variations, and found that the effect of possible distortions to the coils numbered as 9, 10, 11, and 12 and displacements to the coils nubered as 8 and 9 is negligible, but the installation error with inclined coils numbered as 8 and 9 and the EMF direction change would likely affect the efficiency of the PMTs.

Finally, we strongly recommend to the JUNO Collaboration the model of 16 pairs of circular coils for EMF shielding in the JUNO site.

REFERENCES

REFERENCES

Abe, K., Abgrall, N., Aihara, H., Ajima, Y., Albert, J., Allan, D., Amaudruz, P.-A., Andreopoulos, C., Andrieu, B., Anerella, M., Angelsen, C., Aoki, S., Araoka, O., Argyriades, J., Ariga, A., et al. (2011). The T2K Experiment. **Nuclear Instruments and Methods**. A659: 106–135.

Abe, K., Adam, J., Aihara, H., Akiri, T., Andreopoulos, C., Aoki, S., Ariga, A., Assylbekov, S., Autiero, D., Barbi, M., Barker, G., Barr, G., Bartet-Friburg, P., Bass, M., Batkiewicz, M., Bay, F., Berardi, V., et al. (2015a). Neutrino oscillation physics potential of the t2k experiment. **Progress of Theoretical and Experimental Physics**. 2015(4): 043C01.

Abe, K., Aihara, H., Andreopoulos, C., Anghel, I., Ariga, A., Ariga, T., Asfandiyarov, R., Askins, M., Back, J., Ballett, P., Barbi, M., Barker, G., Barr, G., Bay, F., Beltrame, P., et al. (2015b). Physics potential of a long-baseline neutrino oscillation experiment using a j-parc neutrino beam and hyper-kamiokande. **Progress of Theoretical and Experimental Physics**. 2015(5): 053C02.

Abramowitz, M. and Stegun, I. A., editors (1964). Handbook of Mathematical Functions with Formulas, Graphs and Mathematical Tables, volume 55 of *Applied Mathematics Series*. National Bureau of Standards, Washington, D.C. Reprinted by Dover, New York.

Adam, T., An, F., An, G., An, Q., Anfimov, N., Antonelli, V., Baccolo, G., Baldoncini, M., Baussan, E., Bellato, M., Bezrukov, L., Bick, D., Blyth, S., Boarin, S., Brigatti, A., and et al. (2015). JUNO Conceptual Design Report.

Adamson, P., Andreopoulos, C., Arms, K. E., Armstrong, R., Auty, D. J., Ayres, D. S., Baller, B., Barnes Jr., P. D., Barr, G., Barrett, W. L., Becker, B. R., Belias, A., Bernstein, R. H., Bhattacharya, D., Bishai, M., et al. (2008). Measurement of Neutrino Oscillations with the MINOS Detectors in the NuMI Beam. **Physical Review Letters**. 101(13): 131802.

Ahn, J. K., Chebotaryov, S., Choi, J. H., Choi, S., Choi, W., Choi, Y., Jang, H. I., Jang, J. S., Jeon, E. J., Jeong, I. S., Joo, K. K., Kim, B. R., Kim, B. C., Kim, H. S., Kim, J. Y., et al. (2012). Observation of reactor electron antineutrinos disappearance in the reno experiment. **Physical Review Letters**. 108: 191802.

Aiello, S., Leonora, E., Grimaldi, A., Leotta, G., Lo Presti, D., Randazzo, N., Sciliberto, D., and Sipala, V. (2012). Influence of the earth's magnetic field on large area photomultipliers. **IEEE Transactions on Nuclear Science**.

An, F. P., Bai, J. Z., Balantekin, A. B., Band, H. R., Beavis, D., Beriguete, W., Bishai, M., Blyth, S., Boddy, K., Brown, R. L., Cai, B., Cao, G. F., Cao, J., Carr, R., Chan, W. T., et al. (2012). Observation of electron-antineutrino disappearance at daya bay. **Physical Review Letters**. 108: 171803.

Balantekin, A. B. and Haxton, W. C. (2013). Neutrino Oscillations. **Progress in Particle and Nuclear Physics**. 71: 150–161.

Bell, G. B. and Marino, A. A. (1989). Exposure system for production of uniform magnetic fields. **Journal of Bioelectricity**. 8(2): 147–158.

Braibant, S., Giacomelli, G., and Spurio, M. (2012). Particles and Fundamental Interactions: An Introduction to Particle Physics. Springer.

Cherry, S. R., Sorenson, J. A., and Phelps, M. E. (2012). chapter 7 - radiation detectors. In Cherry, S. R., Sorenson, J. A., and Phelps, M. E., editors, **Physics in Nuclear Medicine (Fourth Edition)**, pages 87 – 106. W.B. Saunders, Philadelphia, fourth edition edition.

Ciuffoli, E., Evslin, J., and Zhang, X. (2013). Neutrino mass hierarchy from nuclear reactor experiments. **Physical Review D**. 88: 033017.

de Salas, P. F., Forero, D. V., Ternes, C. A., Tortola, M., and Valle, J. W. F. (2017). Status of neutrino oscillations 2017.

Fengpeng, A., Guangpeng, A., Qi, A., Vito, A., Eric, B., John, B., Leonid, B., Simon, B., Riccardo, B., Avanzini Margherita, B., Jose, B., Anatael, C., Hao, C., Xiao, C., Antonio, C., et al. (2016). Neutrino physics with juno. **Journal of Physics G: Nuclear and Particle Physics**. 43(3): 030401.

Fong, D. C. and Saunders, M. A. (2010). LSMR: an iterative algorithm for sparse least-squares problems. **Computing Research Repository** . abs/1006.0758.

Gando, A., Gando, Y., Ichimura, K., Ikeda, H., Inoue, K., Kibe, Y., Kishimoto, Y., Koga, M., Minekawa, Y., Mitsui, T., Morikawa, T., Nagai, N., Nakajima, K., Nakamura, K., Narita, K., et al. (2011). Constraints on θ_{13} from a three-flavor oscillation analysis of reactor antineutrinos at kamland. **Physical Review D**. 83: 052002.

Goldhaber, M., Grodzins, L., and Sunyar, A. W. (1958). Helicity of neutrinos. **Physical Review Journals Archive**. 109: 1015–1017.

Griffiths, D. J. (2013). Introduction to electrodynamics; 4th ed. Pearson, Boston, MA. Re-published by Cambridge University Press in 2017.

Jollet, C. (2017). The JUNO experiment. **Nuovo Cimento**. C39(4): 318.

Jones, E., Oliphant, T., and Peterson, P. (2001). SciPy: Open source scientific tools for Python. [Online; accessed <today>].

Jr., R. A. S. and Hoff, K. (2001). Characterizing and calibrating a large helmholtz coil at low ac magnetic field levels with peak magnitudes below the earth's magnetic field. **Review of Scientific Instruments**. 72(6): 2769–2776.

Koonin, S. E. and Meredith, D. C. (1990). Computational Physics: Fortran Version.

Krommer, A. R. and Ueberhuber, C. W. (1998). Computational Integration. SIAM, Philadelphia, PA.

Kulikovskiy, V. (2014). Neutrino astrophysics with the ANTARES telescope.

Lawson, C. L., Hanson, Richard J., ., for Industrial, S., and Mathematics, A. (1995). Solving least squares problems. Philadelphia : SIAM, [rev. ed.] edition. "This SIAM edition is an unabridged, revised republication of the work first published by Prentice-Hall, Inc., Englewood Cliffs, New Jersey, 1974"–T.p. verso.

Li, Y. F., Cao, J., Wang, Y., and Zhan, L. (2013). Unambiguous determination of the neutrino mass hierarchy using reactor neutrinos. **Physical Review D**. 88: 013008.

Lu, H. (2017). Status of the JUNO reactor anti-neutrino experiment. **Nuclear and Particle Physics Proceedings**. 287–288: 143–146. The 14th International Workshop on Tau Lepton Physics.

Lu, H. and Baussan, E. (2016). The design of the JUNO veto system.

Lu, H., Baussan, E., and JUNO experiment (2017). The design of the JUNO veto system. **Journal of Physics: Conference Series**. 888(1): 012088.

Malace, S. P., Sawatzky, B. D., and Gao, H. (2013). Studies of single-photoelectron response and of performance in magnetic field of a H8500C-03 photomultiplier tube. **Journal of Instrumentation**. 8: P09004.

Maus, S., Macmillan, S., McLean, S., Hamilton, B., Thomson, A., Nair, M., and Rollins, C. (2010). The us/uk world magnetic model for 2010-2015. Technical report.

Nocedal, J. and Wright, S. J. (2006). Numerical Optimization. Springer, New York, NY, USA, second edition.

Pang, T. (2006). An Introduction to Computational Physics. Cambridge University Press, 2 edition.

Park, P. G., Kim, Y. G., Kalabin, V. N., and Shifrin, V. Y. (2008). AC magnetic flux density standards in the low frequency range. In 2008 Conference on Precision Electromagnetic Measurements Digest, pages 456–457.

Park, P. G., Kim, Y. G., Kim, W.-S., and Shifrin, V. Y. (2010). Ac/dc magnetic flux density standard systems at KRISS. In CPEM 2010, pages 312–313.

Patrignani, C., Agashe, K., Aielli, G., Amsler, C., Antonelli, M., Asner, D., Baer, H., Banerjee, S., Barnett, R., Basaglia, T., Bauer, C., Beatty, J., Belousov, V., Beringer, J., Bethke, S., et al. (2016). Review of Particle Physics. **Chinese Physics C**. C40(10): 100001.

Piessens, R., Kapenga, E. d., Uberhuber, C., and Kahaner, D. (1983). QUADPACK: A Subroutine Package for Automatic Integration. Springer–Verlag.

Press, W. H., Teukolsky, S. A., Vetterling, W. T., and Flannery, B. P. (1993). Numerical Recipes in FORTRAN; The Art of Scientific Computing. Cambridge University Press, New York, NY, USA, 2nd edition.

Schechter, J. and Valle, J. W. F. (1980). Neutrino masses in su(2) $\otimes$ u(1) theories. **Physical Review D**. 22: 2227–2235.

Simpson, J. C., Lane, J. E., Immer, C. D., Youngquist, R. C., and Steinrock, T. (2001). Simple analytic expressions for the magnetic field of a circular current loop.

Stark, P. B. and Parker, R. L. (1995). Bounded-variable least-squares: an algorithm and applications. **Computational Statistics**.

Weisstein, E. W. (2018). Legendre-gauss quadrature. Last visited on 28/2/2018.

Xing-Chen, Y., Bo-Xiang, Y., Xiang, Z., Li, Z., Ya-Yun, D., Meng-Chao, L., Xue-Feng, D., Xuan, Z., Quan-Lin, J., Li, Z., Jian, F., Hai-Tao, C., Wei, H., Shun-Li, N., Jia-Qing, Y., Hang, Z., and Dao-Jin, H. (2015). Preliminary study of light yield dependence on lab liquid scintillator composition. **Chinese Physics C**. C39(9): 096003.

Zhan, L., Wang, Y., Cao, J., and Wen, L. (2008). Determination of the neutrino mass hierarchy at an intermediate baseline. **Physical Review D**. 78: 111103.

Zhou, X., Liu, Q., Han, J., Zhang, Z., Zhang, X., Ding, Y., Zheng, Y., Zhou, L., Cao, J., and Wang, Y. (2015). Spectroscopic study of light scattering in linear alkylbenzene for liquid scintillator neutrino detectors. **The European Physical Journal C**. C75(11): 545.

APPENDICES

APPENDIX A

GAUSSIAN QUADRATURE

The most commonly used orthogonal polynomials as the weight functions of gaussian quadratures consist of 5 polynomials, that is, Gauss-Legendre, Gauss-Chebyshev, Gauss-Laguerre, Gauss-Hermite, and Gauss-Jacobi polynomials (Press et al., 1993). But this dissertation will construct numerical integration quadrature by Gauss-Legendre polynomial. Gauss-Legendre quadrature gives correctly integral polynomials of degree 2N - 1 or less over the interval $[-1, 1]$ with the weight w(y)= 1 (Piessens et al., 1983), where N is a number of the abscissas y_j and weights w_j. Gaussian quadrature formula can be written as

$$\int_{-1}^{1} f(y)dy \approx \sum_{j=1}^{N} w_{yj} f(y_j) \tag{A.1}$$

Normally, any definite integral are in the range from a to b. With the abscissas and weights, the y interval $-1 \leq y \leq 1$ must be mapped onto the x interval $a \leq x \leq b$. Numerical techniques has to replace x of the Eq. A.2 into y in the Eq. A.1.

$$x = -1 + 2\frac{(y-a)}{(b-a)} \tag{A.2}$$

Table A.1 The exact abscissas and weights for order N quadrature

N	$x_(j)$	$w_(j)$
2	$\pm\frac{1}{3}\sqrt{3}$	1
3	0	$\frac{8}{9}$
	$\pm\frac{1}{5}\sqrt{15}$	$\frac{5}{9}$
4	$\pm\frac{1}{35}\sqrt{525-70\sqrt{30}}$	$\frac{1}{36}\left(18+\sqrt{30}\right)$
	$\pm\frac{1}{35}\sqrt{525+70\sqrt{30}}$	$\frac{1}{36}\left(18-\sqrt{30}\right)$
5	0	$\frac{128}{225}$
	$\pm\frac{1}{21}\sqrt{245-14\sqrt{70}}$	$\frac{1}{900}\left(322+13\sqrt{70}\right)$
	$\pm\frac{1}{21}\sqrt{245+14\sqrt{70}}$	$\frac{1}{900}\left(322-13\sqrt{70}\right)$
...	...	...

The Eq. A.1 is hence

$$\int_a^b f(x)dx \approx \sum_{j=1}^{N} w_j f(x_j) \tag{A.3}$$

where

$$w_j = \frac{(b-a)}{2} w_{yj} \tag{A.4}$$

Thereby, The definite integral form is reduced to the form required (Koonin and Meredith, 1990). Furthermore, the abscissas and weights have exactly abscissas as seen in a typical table of Gauss-Legendre rule (Table A.1). The abscissas in Table A.1 are roots of the Legendre polynomial $P_j(x)$, degrees of the abscissas are allowed in sequences 1, 2, 2, 4, 4, 6, 6, 8, 8, 10, 10, 12, and ..., the weights for order n quadrature likewise can be expressed as the roots of polynomials of degrees 1, 1, 1, 2, 2, 3, 3, 4, 4, 5, 5, and so on(Weisstein, 2018).

APPENDIX B

BOUNDED-VARIABLE LEAST SQUARES

As explained in the chapter 2, Bounede-variable least squares (BVLS) is an efficient for the constrained linear least square technique. This part is going into the detail of BVLS which can be determined the solution as the following step,

1. BVLS starts from defining the set of the indices of free components in the unknowns of x, components at their lower bounds, and components at their upper bounds as $\mathcal{F}$, $\mathcal{L}$, and $\mathcal{U}$, respectively. If the initial definition of algorithm is in a fresh initialization, every element of x is set to its lower bound. If the initial definition of algorithm starts using the user's guess about which components of x are within its corresponding bound. The process is going to initialize from setting each component of x whose index is in $\mathcal{F}$ to the average of its lower and upper bounds and putting each component of x whose index is in $\mathcal{L}$ and $\mathcal{U}$ to its corresponding bound.

2. The negative gradient vector (w) is computed by evaluating $A^T(b - Ax)$.

3. After calculating the negative gradient vector, if $\mathcal{F} = \{1, \ldots, n\}$, or, if $w_j \leq 0$ for all $j \in \mathcal{L}$ and $w_j \geq 0$ for all $j \in \mathcal{U}$. If the solution from computing the negative gradient vector is in these conditions, the vector x is therefore the solution of the unknowns. This step is called the Kuhn-Tucker test for convergence.

4. The corresponding component of w is checked essentially. The corresponding component of w is assigned to zero in case the component is not in both

lower and upper bound sets. Consequently, the program turns back to the Kuhn-Tucker test.

5. This step applies the unconstrained least-squares technique for solving z in the condition argmin $\| A'z - b' \|^2$ in case the component of x is not in their lower and their upper bound sets, where b' is the vector less the anticipations of the bound unknowns, that is, $b'_j = b_j - \sum_{k \in \mathcal{L} \cup \mathcal{U}} A_{jk} x_j$. A' is the matrix consisted of those columns of A which indices are elements of $\mathcal{F}$.

6. the program checks each component ($z_{j'}$ of the vector z. If the components is rather than lower bound and less than upper bound of the vector x. The components z is set to equal the components x, the program returns to step 2.

7. If the components of z is out of bounds, the components is used to determine the interpolation constant (α). Set $x_j := x_j + \alpha(z_{j'} - x_j)$ for all component in the free set. If a component of the vector x is more than or equal its upper bound, a component is moved from the free set to the upper bound set. Otherwise, if a component of the vector x is less than or equal its lower bound, a component is moved from the free set to the lower bound set. The program goes to step 5. In case BVLS fails to converge in the condition of the Kuhn-Tucker test, α is forced to change to the deserving bound (Stark and Parker, 1995).

Finally, the program has to find the components of the vector x that is in the condition of the Kuhn-Tucker test.

APPENDIX C

THE CODE FOR GENERATING GEOMETRY

C.1 The points on the coils code

The below commands is written in Python programming language with numpy package for creating a text file of the points on the coils.

```
import numpy as np      #Define numpy package as np.
#Define rotational matrix function
def rot(axis,theta,x,y,z):
    if axis == 'x':          #in clockwise direction.
        deg = np.pi/180
        xx = x
        yy = np.cos(deg*theta)*y - np.sin(deg*theta)*z
        zz = np.sin(deg*theta)*y + np.cos(deg*theta)*z
    elif axis == 'y':
        deg = np.pi/180
        xx = np.cos(deg*theta)*x + np.sin(deg*theta)*z
        yy = y
        zz = -np.sin(deg*theta)*x + np.cos(deg*theta)*z
    elif axis == 'z':
        deg = np.pi/180
        xx = np.cos(deg*theta)*x - np.sin(deg*theta)*y
        yy = np.sin(deg*theta)*x + np.cos(deg*theta)*y
```

```
        zz = z
    return xx,yy,zz
R,H = np.loadtxt('cir_rad_hB2eqh216pd.txt',usecols=(0,1),
unpack=True)  #Read radii and heights from a text file.
#Start for writing in a text file.
f = open('circlecoil.txt','w')
f2 = open('circlecoil2.txt','w')
#*** Define a plane for the slightly distorted coils ****
#plane = 1 is 'YZ' plane; plane = 2 is 'XZ' plane.
plane = 2
sr = 0.3    #A radius of a small half circle.
#*******************************************************
# rotational angle of the coils system:
theta = -32.017 #for the inclination angle.
theta2 = 0 #for the declination angle.
'''rotational angle for the inclination angle with
a rotational error installation.'''
theta2sc = 0
nc = 1
for r,h in zip(R,H):
    # Define the interval points on a coil.
    if nc>=38 and nc<=39:
    #In case of the slightly distorted coils.
        p = 0.001
        ps = 0.1  # For a small half circle.
    else:         # Without installation error.
```

```
            p = 0.001
        tt = 2*np.arcsin(sr/r)
        if nc>=38 and nc<=39:
            '''Create a circular coil with the slightly
distorted coil by given the points in the
Cartesian coordinates.'''
            j = 0
            i = 0
            t = tt/(4*np.pi)
            while t <= 1-tt:
                x = h
                y = r*np.cos(2*np.pi*t)
                z = r*np.sin(2*np.pi*t)
                j += 1
                t += p
            ax = x
            sz = (z-sr)/13
            a=12
            while a >= 1:
                az = sz*a
                ay = np.sqrt(r**2 - az**2)
                j += 1
                a -= 0.5
            print ('done!1\t', '%d\n' % nc)
            if plane == 1:
                while t >= 1-tt and t <= 1:
```

```
            phi = -180
            k = 0
            while phi <= p:
              x = h
              z = sr*np.cos((np.pi/180)*phi)
              y = r*np.cos(tt/2)+np.sqrt(sr**2-z**2)
                j += 1
                k += 1
                phi += k*ps
                i += 1
                t = i*ps
        print ('done!1.1\t', '%d\n' % nc)
elif plane == 2:
        while t >= 1-tt and t <= 1:
          phi = -180
          k = 0
          while phi <= ps:
              x = -sr*np.sin((np.pi/180)*phi)+h
              y = r*np.cos(tt/2)
              z = sr*np.cos((np.pi/180)*phi)
              j += 1
              k += 1
              phi += k*ps
              i += 1
              t = i*ps
j += 1
```

```
'''Write a number of points on each coil to
a text file.'''
f.write('%d\t' % j)
#
'''Write an iterative number of integration to
a text file.'''
f.write('10\n')
i = 0
t = tt/(4*np.pi)
while t <= 1-tt:
    x = h
    y = r*np.cos(2*np.pi*t)
    z = r*np.sin(2*np.pi*t)
    # Call the rotational matrix function.
    xx,yy,zz = rot('y',theta2sc,x,y,z)
    xxx,yyy,zzz = rot('y',theta,xx,yy,zz)
    # Write the points on a text file.
    f.write('%.10f\t' % xxx)
    f.write('%.10f\t' % yyy)
    f.write('%.10f\n' % zzz)
    f2.write('%.10f\t' % xxx)
    f2.write('%.10f\t' % yyy)
    f2.write('%.10f\n' % zzz)
    if i==0:
        x1 = xxx
        y1 = yyy
```

```
            z1 = zzz
        i += 1
        t += p
    ax = x
    sz = (z-sr)/13
    a=12
    while a >= 1:
        az = sz*a
        ay = np.sqrt(r**2 - az**2)
        xx,yy,zz = rot('y',theta2sc,ax,ay,az)
        xxx,yyy,zzz = rot('y',theta,xx,yy,zz)
        f.write('%.10f\t' % xxx)
        f.write('%.10f\t' % yyy)
        f.write('%.10f\n' % zzz)
        f2.write('%.10f\t' % xxx)
        f2.write('%.10f\t' % yyy)
        f2.write('%.10f\n' % zzz)
        a -= 0.5
    print ('done!1\t', '%d\n' % nc)
    if plane == 1:
        while t >= 1-tt and t <= 1:
            phi = -180
            k = 0
            while phi <= ps:
              x = h
              z = sr*np.cos((np.pi/180)*phi)
```

```
                y = r*np.cos(tt/2) + np.sqrt(sr**2-z**2)
                '''The sign between the first and
                second terms of equation y:
                + for outer small half circle and
                - for inner small half circle.'''
                xx,yy,zz = rot('y',theta2sc,x,y,z)
                xxx,yyy,zzz = rot('y',theta,xx,yy,zz)
                f.write('%.10f\t' % xxx)
                f.write('%.10f\t' % yyy)
                f.write('%.10f\n' % zzz)
                f2.write('%.10f\t' % xxx)
                f2.write('%.10f\t' % yyy)
                f2.write('%.10f\n' % zzz)
                k += 1
                phi += k*ps
                i += 1
                t = i*ps
        f.write('%.10f\t' % x1)
        f.write('%.10f\t' % y1)
        f.write('%.10f\n' % z1)
        f2.write('\n')
        f2.write('\n')
        print ('done!1.1\t', '%d\n' % nc)
elif plane == 2:
     while t >= 1-tt and t <= 1:
         phi = -180
```

```
        k = 0
        while phi <= ps:
            x = -sr*np.sin((np.pi/180)*phi) + h
            y = r*np.cos(tt/2)
            z = sr*np.cos((np.pi/180)*phi)
            xx,yy,zz = rot('y',theta2sc,x,y,z)
            xxx,yyy,zzz = rot('y',theta,xx,yy,zz)
            f.write('%.10f\t' % xxx)
            f.write('%.10f\t' % yyy)
            f.write('%.10f\n' % zzz)
            f2.write('%.10f\t' % xxx)
            f2.write('%.10f\t' % yyy)
            f2.write('%.10f\n' % zzz)
            k += 1
            phi += k*ps
            i += 1
            t = i*ps
    f.write('%.10f\t' % x1)
    f.write('%.10f\t' % y1)
    f.write('%.10f\n' % z1)
    f2.write('%.10f\t' % x1)
    f2.write('%.10f\t' % y1)
    f2.write('%.10f\n' % z1)
    f2.write('\n')
    f2.write('\n')
# Create a circular coil without installation error.
```

```
else:
    j = 0
    i = 0
    t = 0
    while t<=1:
        x = h
        y = r*np.cos(2*np.pi*t)
        z = r*np.sin(2*np.pi*t)
        j += 1
        i += 1
        t = i*p
    f.write('%d\t' % j)
    f.write('10\n')
    i = 0
    t = 0
    print ('done!2\t', '%d\n' % nc)
    while t<=1:
        x = h
        y = r*np.cos(2*np.pi*t)
        z = r*np.sin(2*np.pi*t)
        xx,yy,zz = rot('z',theta2,x,y,z)
        xxx,yyy,zzz = rot('y',theta,xx,yy,zz)
        f.write('%.10f\t' % xxx)
        f.write('%.10f\t' % yyy)
        f.write('%.10f\n' % zzz)
        f2.write('%.10f\t' % xxx)
```

```
            f2.write('%.10f\t' % yyy)
            f2.write('%.10f\n' % zzz)
            i += 1
            t = i*p
        f2.write('\n')
        f2.write('\n')
        print ('done!2\t', '%d\n' % nc)
    nc += 1

f.close()
#End for writting in a text file.
f2.close()
```

C.2 The bounds definition for a numerical integration code

The next commands will generate the lower and upper bounds for computing the magnetic fields by using the standard Fortran programming language after the points on the coils were defined.

```
      program position_coils !The name of main program.
      implicit real*8 (a-i,l, o-z)
      INTEGER nmax
      !Define a number of the coils (ncoil2).
      parameter (nmax =13000,ncoil2 = 32)
      real*8 R2(ncoil2),h2(ncoil2),w2(ncoil2),L2(ncoil2),
     1 thec(ncoil2)
      real*8 lwx2(ncoil2,nmax),lwy2(ncoil2,nmax),
```

```
     1 lwz2(ncoil2,nmax),upx2(ncoil2,nmax),
     2 upy2(ncoil2,nmax),upz2(ncoil2,nmax),b(nmax)
      pi = dacos(-1d0)
      !Define EMF in the Cartesian coordinates.
      data (b(j), j=1,3)/0.37988d0,-0.01505d0,0.23772d0/
      !Start for writting in a text file.
      open(22,file='perfecteqh216pryz.txt')
      !Start to read from a text file.
      open(20,file='circlecoil.txt')
      do 1 k=1,ncoil2
*********************************************************
* Read an number of the points on a coil and an        *
* iterative number of integration from a text file.    *
      read(20,*) nwire2,npoint
*********************************************************
*********************************************************
* This step is going to count a number of the points   *
* on each coil again and collects a lower bound and    *
* an upper bound of the points on each coil.           *
*********************************************************
      j=0
        do nw2=1,nwire2
* Read the points in three columns from a text file.   *
      read(20,*) x,y,z
      if (nw2.eq.1) then
      lwx2(ncoil2,nw2+1)=x
```

```
       lwy2(ncoil2,nw2+1)=y
       lwz2(ncoil2,nw2+1)=z
       write(*,*) x,lwx2(ncoil2,nw2),y,lwy2(ncoil2,nw2),z,
      1 lwz2(ncoil2,nw2)
       else if (nw2.ne.1) then
       upx2(ncoil2,nw2)=x
       upy2(ncoil2,nw2)=y
       upz2(ncoil2,nw2)=z
       j= j + 1
       lwx2(ncoil2,nw2+1)=upx2(ncoil2,nw2)
       lwy2(ncoil2,nw2+1)=upy2(ncoil2,nw2)
       lwz2(ncoil2,nw2+1)=upz2(ncoil2,nw2)
       end if
         end do
*************************************************
*************************************************
* Write an number of the points on each coil and *
* an iterative number of integration to          *
* a text file, respectively.                     *
       write(22,*) j,npoint
*************************************************
** End counting a number of the points on each coil **

*************************************************
* This step will write a lower bound and        *
* an upper bound of the points on each coil     *
```

```
* in the Cartesian coordinates for computing  *
* an integration of the Biot-Savart law.      *
***********************************************
        do nw2=1,nwire2
        if (nw2.ne.1) then
*************************************
* The lower and upper bounds         *
* in the x-axis, y-axis, and z-axis. *
*                                    *
      lbx = lwx2(ncoil2,nw2)
      ubx = upx2(ncoil2,nw2)
      lby = lwy2(ncoil2,nw2)
      uby = upy2(ncoil2,nw2)
      lbz = lwz2(ncoil2,nw2)
      ubz = upz2(ncoil2,nw2)
*************************************
          !Write the bounds to a text file.
      write(22,'(6f18.10)') lbx,ubx,lby,uby,lbz,ubz
        end if
        end do
***** End writting the points to a text file *****
    1 end do
      close(20)      !End to read from a text file.
      close(22)      !End for writting in a text file.
      end program
```

APPENDIX D

THE SPHERICAL SURFACE POINTS CODE

This Fortran77 code generate the points on a spherical surface with a radius R. These command return the points in the Cartesian coordinates (x,y,z), the polar (t) and azimuthal (tz) angles.

```
      program Create_spherical_surface  !Start Program.
      implicit real*8 (a-h,n-z)
      !Define the interval between two points.
      ngrid = 2d0
      pi    = dacos(-1d0)
      !Define a radius of a spherical surface.
      R     = 20d0
      tz    = 0d0
      itz   = 0
**************************************************
* Count the number of points on a spherical surface *
* in the Cartesian coordinates.                     *
      open (1, file='surf_sphere.txt')
      open (2, file='surf_sphere3d.txt')
      i = 0
      do while(tz.le.180d0)
      z  =  R*dcos((pi/180d0)*tz)
      t  = 0d0
```

```
      it = 0
      if ((tz.eq.0).or.(tz.eq.180)) then
        x = 0
        y = 0
        i = i + 1
      else
       do while(t.le.(360d0-ngrid))
       x = R*dcos((pi/180d0)*t)*dsin((pi/180d0)*tz)
       y = R*dsin((pi/180d0)*t)*dsin((pi/180d0)*tz)
       it = it + 1
       t = it*ngrid
       i = i + 1
      end do
      end if
      itz = itz + 1
      tz = itz*ngrid
      end do
*     Write the number of the points on                *
*     a spherical surface in a text file.              *
      write(1,*) i
****************** End counting ********************

*******************************************************
* This step writes the points on a spherical surface *
* in the Cartesian coordinates to a text file.       *
      tz    = 0d0    !Initialize a theta angle.
```

```
      itz   = 0
**********************************************
* The condition of a theta angle is that      *
* the theta angles must be less than or       *
* equal 180 degrees.                          *
      do while(tz.le.180d0)
**********************************************
*     Compute a value in the z-axis.          *
      z  =  R*dcos((pi/180d0)*tz)
      t  = 0d0 !Initialize a phi angle.
      it = 0
******************************************
* Here will create the points on the top  *
* and the bottom of a spherical surface.  *
      if ((tz.eq.0).or.(tz.eq.180)) then
        x = 0
        y = 0
*       Write the points to a text file.  *
        write(1,'(1f8.4,3f10.4)') x,y,z,tz,t
        write(2,'(1f8.4,3f10.4)') x,y,z
******************************************

**************************************************
* The generating commands of the excepted points  *
* on the top and the bottom of a spherical surface. *
      else
```

```
*       The condition of a theta angle.                 *
        do while(t.le.(360d0-ngrid))
*       Compute the values in the x-axis, and y-axis.   *
        x = R*dcos((pi/180d0)*t)*dsin((pi/180d0)*tz)
        y = R*dsin((pi/180d0)*t)*dsin((pi/180d0)*tz)
        write(1,'(1f8.4,3f10.4)') x,y,z,tz,t
        write(2,'(1f8.4,3f10.4)') x,y,z
        t = t + ngrid    !Change a phi angle.
        end do  !Finished a loop of the phi angles.
        end if
        write(2,*) ' '
        tz = tz + ngrid    !Change a theta angle.
        end do  !Finished a loop of the theta angles.
*****************************************************


*************** End loop for writting ***************

        close(1)        !Closed a text file.
        close(2)
        end             !End program.
```

APPENDIX E

THE MAGNETIC FIELD CALCULATION AND OPTIMIZATION CODE

E.1 The magnetic field calculation

This program is written in Fortran77 programming language which is used to compute a line integral of the Biot-Savart law in the Cartesian coordinates. This program start from inputting the source points, the field points, and the currents into the Mag subroutine. Then, the Mag subroutine calls the gauleg subroutine to compute numerical integration by using The Gauss-Legendre quadrature formula. So, the Mag subroutine returns the magnetic fields in the Cartesian coordinates of a source point. This program iterate until the $nline^{th}$ source point.

```
      program surfpert41
      implicit real*8 (a-h,l,o-z)
      INTEGER nmax,ncoil1,ncoil2
      !Specify the number of coils (ncoil1).
      parameter (nmax =33000, ncoil1 = 32)
      real*8 R1(ncoil1),h1(ncoil1)
      real*8 Bx1(nmax,ncoil1),By1(nmax,ncoil1),
     1 Bz1(nmax,ncoil1),I1(ncoil1),Bsumx1(nmax)
      real*8 Bsumy1(nmax),Bsumz1(nmax),Bsum1(nmax)
      real*8 x(nmax),y(nmax),z(nmax),b(nmax)
      pi    = dacos(-1d0)
```

```
      !The EMF in the Cartesian coordinates.
      data (b(m), m=1,3)/0.37988d0,-0.01505d0,0.23772d0/

******** Label the currents from a text file. **********
      open(26,
     1 file='Ieqh516p395.txt')
      do k=1, ncoil1
       read(26,*) I1(k)
      end do
      close(26)
*****************************************************

!Input the datas from the file which is labeled by the 20
      open(20,file='surf_sphere_pts41.txt')
!ntplot is the integer for designating a type of a plot.
      read(20,*) ntplot
      if (ntplot.eq.1) then
      !In case a spherical surface plot.
      !A number of the points for plotting (nline).
       read(20,*) nline
       open(1, file=
     1 'sphe_magsumJUNOB241ryeqh516p395cury.txt')
       open(11, file=
     1 'hist_magsumJUNOB241ryeqh516p395cury.txt')
      else if (ntplot.eq.2) then
      !In case a cylindrical surface plot.
```

```
        read(20,*) nline
        open(2, file='cylin_magsumJUNOB2.txt')
        open(12, file='hist_magsumJUNOB2.txt')
      else
      !In case a line plot.
        read(20,*) nline
        open(3, file='magtest516phcr20.txt')
      end if
*************************************************
* This loop is for computing magnetic fields of *
* the field points from an input file.          *
      do j=1,nline
* Here is the commands for inputting            *
* the field points                              *
      if (ntplot.eq.1) then
       read(20,*) x(j),y(j),z(j),theta,t,stz
      else if (ntplot.eq.2) then
       read(20,*) x(j),y(j),z(j),t,h,R
      else
       read(20,*) x(j),y(j),z(j)
      end if
      rx        = x(j)
      ry        = y(j)
      rz        = z(j)
      Bsumx1(j) = 0d0
      Bsumy1(j) = 0d0
```

```
      Bsumz1(j) = 0d0
* The file with labeled 101 is the points       *
* on the coils.                                  *
      open(101,file='perfecteqh516pp.txt')
      do k=1,ncoil1
* Read the number of the points on              *
* the coils(nwire1) and the number of summation *
* in a numerical integration(npoint).           *
      read(101,*) nwire1,npoint
      cur1 = I1(k)
* In the optimization case, the cur1 is 1d0.    *
      Bxi1=0d0
      Byi1=0d0
      Bzi1=0d0
************************************************
* Here is the loop for evaluating               *
* a magnetic field in a point from a coil.      *
      do 101 nw1=1,nwire1
* Read to input the lower and upper bounds      *
* in the Cartesian coordinates for              *
* an integration from the file with             *
* labeled 101.                                  *
      read(101,*) lbx1,ubx1,lby1,uby1,lbz1,ubz1
      rad1 = 0d0
* Call the magnetic field calculation subroutine *
      call Mag(npoint,rx,ry,rz,cur1,lbx1,ubx1,lby1,
```

```
     1 uby1,lbz1,ubz1,rad1,Bxi1,Byi1,Bzi1,Bxg1,Byg1,
     2 Bzg1)
  101    end do
* End the loop for evaluating a magnetic field   *
* in a point from a coil.                         *
       Bx1(j,k) = Bxg1
       By1(j,k) = Byg1
       Bz1(j,k) = Bzg1
* Sum the magnetic fields from the coils         *
* in this system of a field point.                *
       Bsumx1(j) = Bsumx1(j) + Bx1(j,k)
       Bsumy1(j) = Bsumy1(j) + By1(j,k)
       Bsumz1(j) = Bsumz1(j) + Bz1(j,k)
* In the optimization, the above commands for    *
* summing the magnetic fields is disappeared.    *
       end do
       close(101)
* Finished for evaluating a magnetic field of    *
* a field point from the coils system.            *
*      The resultant of EMF.                      *
       Ber = dsqrt(b(1)**2d0+b(2)**2d0+b(3)**2d0)
*A resultant of a magnetic field of a field point. *
       Bsum1(j) = dsqrt((Bsumx1(j))**2d0 +
     1 (Bsumy1(j))**2d0 + (Bsumz1(j))**2d0)
       res = dsqrt((Bsumx1(j)-b(1))**2d0+
     1 (Bsumy1(j)-b(2))**2d0+(Bsumz1(j)-b(3))**2d0)
```

```
* The following conditions is commands for          *
* writting the datas from a magetic field           *
* calculation.                                      *
      if (ntplot.eq.1) then
      write(1,'(1f8.4,1f10.4,6f15.8)') theta,t,Bsumx1(j),
     1 Bsumy1(j),Bsumz1(j),Bsum1(j),res,Ber
      write(11,'(1f8.4)') res
      else if (ntplot.eq.2) then
        write(2,'(1f8.4,2f10.4,6f15.8)') t,h,R,Bsumx1(j),
     1  Bsumy1(j),Bsumz1(j),Bsum1(j),res
      write(12,'(1f8.4,1f10.4,7f15.8)') res
      else
       write(3,'(1f15.8,1f15.8,6f15.8)') x(j),y(j),z(j),
     1  Bsumx1(j),Bsumy1(j),Bsumz1(j),Bsum1(j)
      end if
* In the optimization, the above commands is        *
* replaced by the following commands,               *
* write(1,'(50f20.10)') (Bx1(j,k), k=1,ncoil1),     *
* write(1,'(50f20.10)') (By1(j,k), k=1,ncoil1),     *
* write(1,'(50f20.10)') (Bz1(j,k), k=1,ncoil1)      *
*   These commands create a rectangular matrix      *
* with the ncoil1 columns in each loop.             *
* Each component is a generated magnetic field      *
* from  a coil.                                     *
* The commands for writting the EMF in a text file  *
* also needs to add it, the commands can be         *
```

```
* written as                                                    *
* do m=1,3                                                     *
* vecb = b(m)                                                  *
* write(22,'(f15.10)') vecb                                    *
* end do                                                       *
* The file with labeled 22 is written the three                *
* components of  EMF in each loop and one column.              *
      if (ntplot.eq.1) then
       if (t.eq.360d0) then
        write(1,*) ' '
       end if
      else if (ntplot.eq.2) then
       if (t.eq.360d0) then
        write(2,*) ' '
       end if
      else
       if (x(j).eq.ncols) then
        !write(3,*) ' '
       end if
      end if
      end do
* Finished for computing the magnetic fields                   *
* all of the spherical surface points.                         *
***************************************************************
      close(1)
      close(11)
```

```
      close(2)
      close(12)
      close(3)
      end program
*****************************************************
* This is the subroutine for computing a magnetic   *
* field from any arbitrary shape.                   *
      subroutine Mag(npoint,rox,roy,roz,I,lbx,ubx,lby,
     1 uby,lbz,ubz,R,Bsumx,Bsumy,Bsumz,Bsumxg,
     2 Bsumyg,Bsumzg)
      implicit real*8 (a-i,k-l,o-z)
      real*8  mu,k
      dimension xri(50000),wrix(50000),yri(50000),
     1 wriy(50000),zri(50000),wriz(50000)
* Define the constants for the Biot-Savart law.     *
      pi = dacos(-1d0)
      mu = 4d0*pi*1d-7
      k  = (mu*I)/(4d0*pi)
      l  = 1d0/2d0
      Gs = 1d4
* Call the Gauss-Legendre quadrature formula        *
* which is the subroutine for integrating           *
* a magnetic field.                                 *
      call gauleg(lbx,ubx,xri,wrix,npoint)
      call gauleg(lby,uby,yri,wriy,npoint)
      call gauleg(lbz,ubz,zri,wriz,npoint)
```

```
      do j=1,npoint
* The below commands is the source points with      *
* a current\-carrying in the counter\-clockwise     *
* direction.                                        *
      if (R.eq.0d0) then
      !The source points of a straight line.
        cx  = xri(j)
        cy  = yri(j)
        cz  = zri(j)
        dx = wrix(j)
        dy = wriy(j)
        dz = wriz(j)
      else
      !The source points of a circle.
        if(lbx.eq.ubx) then
        !A circular coil on the x-axis.
          yri(j) = zri(j)
          cx = xri(j)
          cy = R*dcos(yri(j))
          cz = R*dsin(zri(j))
          dx = wrix(j)
          dy = -cz*wriy(j)
          dz = cy*wriz(j)
        else if(lby.eq.uby) then
        !A circular coil on the y-axis.
          xri(j) = zri(j)
```

```
            cx = R*dsin(xri(j))
            cy = yri(j)
            cz = R*dcos(zri(j))
            dx = cz*wrix(j)
            dy = wriy(j)
            dz = -cx*wriz(j)
          else if(lbz.eq.ubz) then
          !A circular coil on the z-axis.
            yri(j) = xri(j)
            cx  = R*dcos(xri(j))
            cy  = R*dsin(yri(j))
            cz  = zri(j)
            dx = -cy*wrix(j)
            dy = cx*wriy(j)
            dz = wriz(j)
          end if
        end if
        x  = rox - cx
        y  = roy - cy
        z  = roz - cz
        rt3 = (x**2d0+y**2d0+z**2d0)**(3d0/2d0)

* The general form of the magnetic field in          *
* the x-axis.                                        *
        wfxi = k*(z*dy - y*dz)/rt3
        Bsumx = Bsumx + wfxi
```

```
* The general form of the magnetic field in          *
* the y-axis.                                        *
      wfyi = k*(x*dz - z*dx)/rt3
      Bsumy = Bsumy + wfyi
* The general form of the magnetic field in          *
* the z-axis.                                        *
      wfzi = k*(y*dx - x*dy)/rt3
      Bsumz = Bsumz + wfzi
      end do
* Finished for computing a magnetic field in only    *
* one arbitrary shape.                               *
*     Change from the Tesla to the Gauss.            *
      Bsumxg = Bsumx*Gs
      Bsumyg = Bsumy*Gs
      Bsumzg = Bsumz*Gs
      return
      end subroutine

*****************************************************
* The Gauss-Legendre quadrature formula subroutine.  *
* This subroutine is from the numerical recipes in   *
* Fortran 77 online book.                            *
* (http://www.aip.de/groups/soe/local/numres/)       *
      SUBROUTINE gauleg(x1,x2,x,w,n)
*****************************************************
      INTEGER n
```

```
      REAL*8 x1,x2,x(n),w(n)
      DOUBLE PRECISION EPS
      PARAMETER (EPS=3.d-14) !The relative precision.
*****************************************************
* Given the lower and upper limits of integration   *
* x1 and x2, and given n, this routine returns      *
* arrays x(1:n) and w(1:n) of length n, containing  *
* the abscissas and weights of the GaussLegendre    *
*      n-point quadrature formula.                  *
*****************************************************
      INTEGER i,j,m
      DOUBLE PRECISION p1,p2,p3,pp,xl,xm,z,z1
*                                                   *
* The roots are symmetric in the interval, so we    *
* only have to find half of them.                   *
      m=(n+1)/2
      xm=0.5d0*(x2+x1)
      xl=0.5d0*(x2-x1)
*                                                   *
      do 12 i=1,m        !Loop over the desired roots.
            z=cos(3.141592654d0*(i-.25d0)/(n+.5d0))
* Starting with the above approximation to the ith  *
* root, we enter the main loop of refinement by     *
* 'Newtons method.                                  *
    1       continue
                p1=1.d0
```

```
                p2=0.d0
                do 11 j=1,n
* Loop up the recurrence relation to get the        *
* Legendre polynomial evaluated at z.               *
                  p3=p2
                  p2=p1
                  p1=((2.d0*j-1.d0)*z*p2-(j-1.d0)*p3)/j
   11           enddo
* p1 is now the desired Legendre polynomial.        *
* We next compute pp, its derivative, by            *
* a standard relation involving also p2, the        *
* polynomial of one lower order.                    *
                pp=n*(z*p1-p2)/(z*z-1.d0)
                z1=z
                z=z1-p1/pp      !'Newtons method.
            if(abs(z-z1).gt.EPS)goto 1
* Scale the root to the desired interval, and put   *
* in its symmetric counterpart Compute the weight   *
* and its symmetric counterpart.                    *
            x(i)=xm-xl*z
            x(n+1-i)=xm+xl*z
            w(i)=2.d0*xl/((1.d0-z*z)*pp*pp)
            w(n+1-i)=w(i)
   12 enddo
      return
      END SUBROUTINE
```

E.2 The current optimization code

After magnetic calculation in the E.1, the matrices of the magnetic fields in the cartesian coordinates and the EMF are used to find the currents by using bvls method and the below commands of Python which is done by the lsq_linear function of the Scipy package.

```
import numpy as np
# Use lsq_linear function from the optimization submodule.
from scipy.optimize import lsq_linear
# Declares A as m by n matrix
A = np.genfromtxt('ma.txt')
# Gives b as the vector with m elements
b = np.genfromtxt('mb.txt')
''' res is the result from lsq_linear function and returns
the values by typing res.x. This program computes by using
bvls method with the minimized variable as 10.322 and
the maximized variable as 141.06. '''
res = lsq_linear(A, b, bounds=(10.322,141.06),
method='bvls', lsmr_tol='auto', verbose=1)
IB1 = open('I.txt','w')
for re in res.x:
# This loop writes the results from res with 3 decimals.
    IB1.write('%.3f\n' % re)
IB1.close()
```

CURRICULUM VITAE

Name: Julanan Songwadhana

Date of Birth: May 11, 1993

Place of Birth: Chanthaburi, Thailand

Education:

- B. Sc. Department of Physics, Srinakharinwirot University, Thailand, 2015.

Publications

Grants and Fellowships: Scholarship Awarding to Graduate Students Whose Lecturers Are Awarded Research Funding by Outside Sources (OROG)